Search for Heavy Long-Lived Charged Particles with the ATLAS detector in pp collisions at $\sqrt{S} = 7$ TeV

Research thesis

Submitted in Partial Fulfillment of The
Requirements for the
Degree of Doctor of Philosophy

Shikma Bressler

Submitted to the Senate of
the Technion - Israel Institute of Technology

Iyar, 5771 Haifa June 2011

The Research Thesis Was Done Under The Supervision of Prof. Shlomit Tarem in the Faculty of Physics.

I am deeply grateful to Prof. Shlomit Tarem for her devoted guidance and support in every aspect.

I would like to thank my good friends and colleagues Enrique Kajomovitz and Sofia Vallecorsa. Working with them was a pleasure.

I would like to thank the HEP group at the Technion for the friendly working atmosphere and the kind help in everything that was needed.

The help of Prof. Yael Shadmi and Iftah Galon concerning the theoretical aspects of this work is highly appreciated.

The Generous Financial Help Of The Pollak Foundation, the Gutwirth Foundation and Technion Is Gratefully Acknowledged.

Finally, I would like to thank my friends and family for their love and support. Without them, walking along this way would mean much less.

Contents

List of Figures

List of Tables

Abstract

A search for long-lived charged particles reaching the muon spectrometer is performed using a data sample of 37 pb^{-1} from pp collisions at $\sqrt{s} = 7$ TeV collected by the ATLAS detector at the LHC. No excess is observed above the estimated background. Stable $\tilde{\tau}$ sleptons are excluded at 95% CL up to a mass of 136 GeV, in GMSB models with $N_5 = 3$, $m_{\mathrm{messenger}} = 250$ TeV, $\mathrm{sign}(\mu) = 1$ and $\tan\beta = 5$. Electroweak production of sleptons is excluded up to a mass of 110 GeV. Gluino R-hadrons in a generic interaction model are excluded up to masses of 530 GeVto 544 GeVdepending on the fraction of R-hadrons produced as $\tilde{g}$-balls.

List of abbreviations

LLP	Long Lived Particle
SUSY	Super Symmetry
LHC	Large Hadron Collider
ID	Inner Detector
MS	Muon Spectrometer
GMSB	Gauge Mediated SUSY Breaking
SM	Standard Model
LSP	Lightest SUSY Particle
NLSP	Next to Lightest SUSY Particle
MDT	Monitor Drift Tube
RPC	Resistive Plate Chamber
TGC	Thin Gap Chamber
CSC	Cathod Strip Chamber

1 Introduction

Heavy long-lived particles (LLPs), with decay length longer than tens of meters, are predicted in a range of theories which extend the Standard Model. Supersymmetry (SUSY) [1] models allow for meta-stable sleptons ($\tilde{l}$), squarks ($\tilde{q}$) and gauginos. Heavy LLPs produced at the Large Hadron Collider (LHC) [2] could travel with velocity significantly lower than the speed of light. These particles can be identified and their mass, m, measured from velocity, β, and momentum, p, measurements using the relation $m = p/\gamma\beta$. Two different searches are presented in this thesis, both use time-of-flight to measure β, and are optimized for the somewhat different experimental signatures of sleptons and R-hadrons.

Long-lived sleptons would interact like heavy muons, releasing energy by ionization as they pass through the ATLAS detector. A search for long-lived sleptons identified in both the inner detector (ID) and in the muon spectrometer (MS) is performed. The results are interpreted in the framework of Gauge Mediated SUSY breaking (GMSB) [3, 4] with the light $\tilde{\tau}$ as the LLP. If the mass difference between the other light sleptons and the light $\tilde{\tau}$ is very small, they may also be long-lived, otherwise the other light sleptons decay to the $\tilde{\tau}$.

Coloured LLPs ($\tilde{q}$ and $\tilde{g}$) would hadronize forming R-hadrons, bound states composed of the LLP and light quarks or gluons. They may emerge as neutral states from the pp collision and become charged by interactions with the detector material, arriving as charged particles in the MS. A dedicated search for R-hadrons is performed in which candidates are required to have MS signals while ID and Calorimeter signals are used if available. The ability to find R-hadrons without requiring an ID track makes this analysis complementary to a previous ATLAS paper searching for R-hadrons [5], that was based on ID and calorimeter signals without any requirement on the MS. In particular, the MS based search presented here is more sensitive to models with larger $\tilde{g}$-ball fractions. The results of this analysis are interpreted in the framework of Split SUSY [6, 7] with the $\tilde{g}$ as the LLP.

This thesis is organized as follows; a brief theoretical motivation is given in 2. The ATLAS detector is described in section 3, the focus is on the time measurement, trigger system and reconstruction algorithms, which are relevant to the LLP search. Section 4 describes the expected signature of LLPs in ATLAS. The strategy of the measurement is introduced in section 5. Section 6 describes the data and simulated samples used in this work. Section 7 describes the reconstruction of LLPs. The difference between slepton reconstruction and R-hadron reconstruction is explained. The β measurement method is described in section 8. Signal selection and associated efficiency are discussed in section 9. Section 10 describes the background estimation method. The systematic uncertainties are estimated in section 11. The results are interpreted into limits in the framework of GMSB and Split-SUSY in section 12.

2 Theoretical motivation

The Standard Model (SM) is the current model of the fundamental particles and their interactions. Since the early 1970s thousands of experiments at energy ranges of hundreds of GeV have been preformed with no confirmed deviation from the SM predictions. However, different phenomena like the gravitational interaction, the nature of the dark matter or the so-called hierarchy problem [8] are not solved by the SM. In order to account for these phenomena, the SM has to be extended.

A large range of theories extending the SM predict the existence of heavy LLPs, these are summarized in [9] . The results of the analysis presented in this thesis are interpreted in the framework of two of these models, gauge mediated SUSY breaking (GMSB) and split SUSY described below.

2.1 Gauge Mediated SUSY Breaking

In GMSB models the SUSY breaking is mediated by gauge interactions [10]. The model assumes that supersymmetry is broken with a scale $\sqrt{F}$ in a sector of the theory which contains heavy non-SM particles. This sector then couples to a set of particles with SM interactions, called messengers, which have a mass of order $m_{\text{messenger}}$. These messengers are taken to be complete representations of SU(5) so as to preserve the coupling constant unification of the Minimal Supersymmetric Standard Model. The mass splitting between the super-partners in the messenger multiplets is controlled by $\sqrt{F}$. One loop diagrams involving these messenger fields, then give mass to super-partners of the gauge bosons of the SM, and two loops diagrams give mass to the super-partners of the quarks and leptons of the SM..

The lightest SUSY particle (LSP) in GMSB models is the gravitino. The next to lightest SUSY particle (NLSP) can be either neutral (the lightest $\tilde{\chi}^0$) or charged. If the NLSP is charged, it is likely to be the right handed slepton ($\tilde{\ell}_R$). While the sleptons $\tilde{e}_R$ and $\tilde{\mu}_R$ are almost mass degenerate, the τ Yukawa coupling may lower the lighter $\tilde{\tau}$ mass through both renormalization group evolution and left-right mixing. These effects are enhanced for large tanβ. The lightest scalar is thus the lighter $\tilde{\tau}$, which is predominantly $\tilde{\tau}_R$. Nevertheless, co-NLSP scenarios where the three light sleptons are almost degenerate, and the decay of the $\tilde{e}_R$ and $\tilde{\mu}_R$ to the $\tilde{\tau}$ is suppressed are also possible. In general, GMSB models are characterized by six parameters:

1. $\mathbf{\Lambda} = \frac{\mathbf{F}}{\mathbf{m}_{\text{messenger}}}$: the SUSY breaking mass scale.
2. $\mathbf{m}_{\text{messenger}}$: the messenger mass.
3. $\mathbf{N}_5$: the number of messenger fields.

4. tanβ : the ratio of the vacuum expectation values of the two Higgs fields.
5. signμ : the sign of the μ term.
6. C_{grav} : the scale factor for the gravitino mass which determines the NLSP life time ($\tau_{NLSP} \sim C^2_{\text{grav}}$).

In the analysis presented in this thesis we considered C_{grav} of $\mathcal{O}(10^3)$ which ensures that the NLSP is long lived with decay length much larger than the length of the detector. Since we look for charged particles, we are interested in cases where $m_{\tilde{\tau}} < m_{\tilde{\chi}^0}$. The ratio between $m_{\tilde{\tau}}$ and $m_{\tilde{\chi}^0}$ is affected by N_5, $m_{\text{messenger}}$ and tanβ. At the messenger scale, $m_{\tilde{\ell}} \propto \sqrt{N_5}$ and $m_{\tilde{\chi}^0} \propto N_5$ so that large N_5 favors the $\tilde{\tau}$ NLSP scenario. The dependance on $m_{messenger}$ is due to the renormalization group evolution which increases $m_{\tilde{\tau}}$ with respect to $m_{\tilde{\chi}^0}$. Large tanβ reduces the mass of the lightest $m_{\tilde{\tau}}$ through the left-right mixing.

Figure 1 [11] shows contours of $m_{\tilde{\tau}_R} = m_{\tilde{\chi}^0}$ in the ($m_{\text{messenger}}$,N_5) plane for various tanβ. The masses are evaluated at the MSSM scale, $m_{\text{MSSM}} = 1$ TeV. In the region above the contour, the $\tilde{\tau}_R$ is the NLSP while below it the $\tilde{\chi}^0$ is the NLSP. As emphasized in [11], $m_{\tilde{\tau}_R}$ and $m_{\tilde{\chi}^0}$ are only approximately the physical lightest $\tilde{\tau}$ and lightest $\tilde{\chi}^0$ since additional contributions, in particular left-right mixing effects with large tanβ, may lower the mass of the lightest $\tilde{\tau}$. As can be seen, for $N_5 \geq 2$ the lightest $\tilde{\tau}$ is the NLSP for a wide range of the parameter space.

2.1.1 GMSB event at the LHC

The weak coupling of the gravitino to the other particles implies that only the NLSP decays to the gravitino[1]. As a result, not only that the NLSP gains a long life time, but it also appears in every GMSB decay chain, and at least two NLSPs exist in each (R-parity conserving) GMSB event.

GMSB events in the LHC can be either strongly or electro-weakly produced. In a strongly produced event two $\tilde{q}$'s or $\tilde{g}$'s emerge from the interaction point (IP), giving rise to two different decay chains. As illustrated in figure 2 (left), each decay chain produces quarks and ends with a decay to a $\tilde{\tau}$ ($\tilde{\ell}$) and a τ (ℓ), so that strongly produced GMSB event is expected to be crowded, with at least two $\tilde{\tau}$'s, two associated leptons and additional energetic jets. An example decay chain of an electro-weakly produced GMSB event is illustrated in figure 2 (right). Similarly to the strong production case, at least two $\tilde{\tau}$'s and two associated leptons are expected in each event. However, electro-weakly produced GMSB events are expected to be less crowded with low hadronic activity.

---

[1] In the co-NLSP scenario the three light sleptons decay to the gravitino

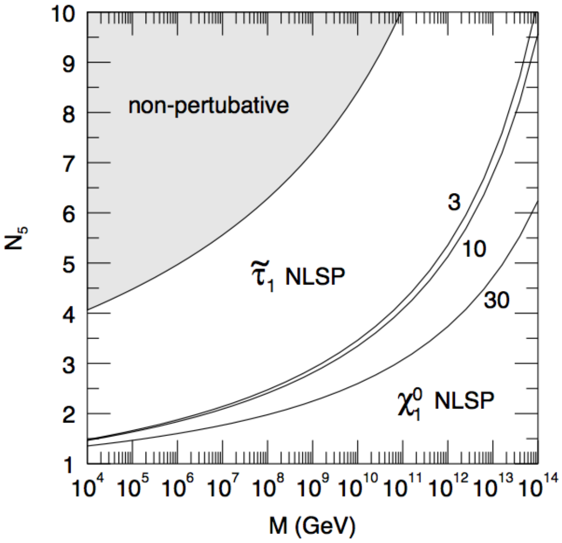

Figure 1: Contours of $m_{\tilde{\tau}_R} = m_{\tilde{\chi}^0}$ in the $(m_{\mathrm{messenger}}, N_5)$ plane for various tanβ. The masses are evaluated at the MSSM scale, $m_{\mathrm{MSSM}} = 1$ TeV. In the region above the contour, the $\tilde{\tau}_R$ is the NLSP while below it the $\tilde{\chi}^0$ is the NLSP.

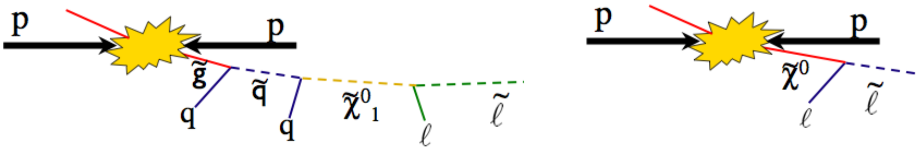

Figure 2: Left: an illustration of a decay chain of a strongly produced GMSB event. Right: an illustration of a decay chain of an electro-weakly produced GMSB event.

2.2 Split SUSY

In split SUSY [6, 7], the masses of the super-symmetric fermions are assumed to be at the TeV range, while the masses of all the scalars, apart from a single Higgs boson are assumed to be very high. If R-parity is conserved, the decay of the colored $\tilde{g}$ involves a heavy $\tilde{q}$ and is therefore suppressed. As a result, the $\tilde{g}$ can become long lived.

Since $\tilde{g}$ is a colored particles, if it is produced, it will hadronize into an R-hadrons - a bound state of $\tilde{g}$ and additional SM particles. An R-hadrons can be R-baryon ($\tilde{g}qqq$), R-meson ($\tilde{g}q\overline{q}$) or a $\tilde{g}$-ball ($\tilde{g}g$). The fraction of R-hadrons of each type is unknown and changes with the hadronization model [12] assumed.

2.2.1 split SUSY event at the LHC

Two $\tilde{g}$'s are strongly produced close to threshold, in each split SUSY event. Each $\tilde{g}$ hadronizes to form different R-hadron. The relatively small amount of additional hadrons produced in the interaction point (IP) account for charge conservation, so that the charge of the two produced R-hadrons is independent.

Therefore, split SUSY events in the LHC are characterized by small number of tracks, mainly of low p_{T} hadrons. In order to be discovered by the analysis presented in this thesis, at least one of the R-hadron has to be charged in the MS.

3 The ATLAS detector

The ATLAS detector [13] is a multipurpose particle physics apparatus with a forward-backward symmetric cylindrical geometry and near 4π coverage in solid angle [2]. The inner detector (ID) consists of a silicon pixel detector, a silicon microstrip detector, and a transition radiation tracker. The ID is surrounded by a thin superconducting solenoid providing a 2 T magnetic field, and by high-granularity liquid-argon sampling electromagnetic calorimeters. An iron scintillator tile calorimeter provides hadronic coverage in the central rapidity range. The end-cap and forward regions are instrumented with liquid-argon calorimetry for both electromagnetic and hadronic measurements. The muon spectrometer (MS) surrounds the calorimeters and consists of three large superconducting air-core toroids each with eight coils, a system of precision tracking chambers, and detectors for triggering. We

---

[2] ATLAS uses a right-handed coordinate system with its origin at the nominal interaction point in the centre of the detector and the z-axis coinciding with the axis of the beam pipe. The x-axis points from the interaction point to the centre of the LHC ring, and the y-axis points upward. Cylindrical coordinates (r, ϕ) are used in the transverse plane, ϕ being the azimuthal angle around the beam pipe. The pseudorapidity is defined in terms of the polar angle θ as $\eta = -\ln\tan(\theta/2)$.

describe the components of particular importance to this analysis in more detail below.

3.1 Bunch crossing identification

The LHC is designed to operate at a 40 MHz rate. Since the distance from the interaction point to the outer most parts of the ATLAS detector is over 20 m, up to three events may co-exist in the detector. To match correctly event fragments from different sub detectors, bunch crossing identification is crucial. The bunch crossing identification is based on time measurement and is calibrated to ensure that the signals left by all the particles originating together at the interaction point and traveling at the speed of light will be associated with the same bunch crossing.

3.2 The ATLAS trigger

ATLAS has a trigger system to reduce the data taking rate from 40 MHz to $\sim$ 100Hz, designed to keep the events that are potentially the most interesting. The first level trigger [14] selection is done by custom hardware and identifies a detector region and a bunch crossing for which a trigger element was found. The second level trigger [15] is performed by dedicated software, making its decision based on data acquired from the bunch crossing and Region of Interest found at level-1. The event filter [15] uses the complete event data to refine the selection of level-2.

3.3 The Muon Spectrometer

The ATLAS Muon Spectrometer (MS) [16] forms the outer part of the ATLAS detector and is designed to detect charged particles exiting the barrel and end-cap calorimeters and to measure their momentum in the pseudorapidity range $|\eta| < 2.7$. It is also designed to trigger on these particles in the region $|\eta| < 2.4$. Precision-tracking chambers in the barrel region are located between and on the eight coils of the superconducting barrel toroid magnet, while the end-cap chambers are in front and behind the two end-cap toroid magnets.

The chambers in the barrel are arranged in three concentric cylindrical shells around the beam axis at radii of approximately 5 m, 7.5 m, and 10 m. In the two end-cap regions, muon chambers form large wheels, perpendicular to the z-axis and located at distances of $|z| = 7.4$ m, 10.8 m, 14 m, and 21.5m from the interaction point.

3.3.1 The muon detectors

The precision momentum measurement is performed by the Monitored Drift Tube chambers (MDTs). These chambers consist of three to eight layers of drift tubes, operated at an absolute pressure of 3 bar, which achieve an average resolution of 80 μm per tube, or about 35 μm per chamber. In the forward region ($2 < |\eta| < 2.7$), Cathode-Strip Chambers (CSC) are used in the innermost tracking layer due to their higher rate capability and time resolution. The CSCs are multiwire proportional chambers with cathode planes segmented into strips in orthogonal directions.

The precision-tracking chambers are complemented by a system of fast trigger chambers capable of delivering track information within a few tens of nanoseconds after the passage of the particle. In the barrel region ($|\eta| < 1.05$), Resistive Plate Chambers (RPC) perform this task, while in the end-cap ($1.05 < |\eta| < 2.4$) this is done by Thin Gap Chambers (TGC). The trigger chambers measure both coordinates of the track, one in the bending (η) plane and one in the non-bending (ϕ) plane.

Time measurement in the Muon Drift Tubes: The MDT chambers are composed of layers of grounded tubes filled with gas. In the middle of each tube there is a wire to which a high voltage is applied. When a charged particle passes through a tube it ionizes the gas, and the ionized electron drifts toward the wire. The hit position is obtained from the particle drift time, measured with a granularity of 0.8 ns, using a known relation between the drift distance and the drift time, $R = R(t_{\mathrm{drift}})$. The result is a ring of radius R around the wire. A segment is reconstructed as a line tangent to the rings in the different layers. The drift time is estimated by subtracting the expected time-of-flight, t_0, from the measured signal time. The expected t_0 is based on particles passing the detector at the speed of light. Slow particles have a longer time-of-flight, and therefore, when this is not taken into account, the measured radius is larger than the true one. Larger radii may result in either badly fitted segment or wrong direction of the segment.

Time measurement in the Resistive Plate Chambers: In the barrel of the MS, RPC chambers have an intrinsic time resolution of $\sim$1 ns while the digitized signal is sampled with a 3.12 ns granularity, allowing a measurement of the time-of-flight. When a charged particle passes through an RPC chamber two signals are generated; one measuring its time and position in the ϕ direction and the other measuring it time and position in the η direction. The time measurement includes the time-of-flight and in addition the propagation time along the strip from the point where the particle passed the detector to the readout electronics. Once the hit positions in both directions are known, the propagation time can be subtracted.

3.3.2 Muon trigger

The muon trigger system is designed to select events containing muons with p_{T} above a certain threshold. It is important to note that any particle arriving as charged in the MS, not necessarily a muon, may be identified as a muon trigger object. The analysis presented in this thesis is based on events collected by two types of muon trigger chains. The first type requires MS tracks to be matched with ID tracks at level-2 and the EF, and estimates the candidate p_{T} based on both systems. The second type only uses the MS, so as not to lose candidates which may not have reconstructed tracks in the ID.

3.3.3 Muon reconstruction

In ATLAS, muons are reconstructed using the MDTs, precision muon chambers, in combination with the RPC, TGC and CSC sub-detectors. ATLAS employs a variety of strategies for identifying and reconstructing muons. The direct approach is to reconstruct standalone muons by finding tracks in the MS and then extrapolating these to the beam line. Combined muons are found by matching standalone muons to nearby ID tracks and then combining the measurements from the two systems. Muons are also found by extrapolating ID tracks to the spectrometer detectors, searching for nearby hits and reconstructing the muon from the ID track and muons signals. Calorimeter tagging algorithms tag ID tracks as muons using the presence of a minimum ionizing signal in calorimeter cells. Muon reconstruction in ATLAS and it's efficiency is described in [17].

3.4 The tile calorimeter

The ATLAS tile calorimeter is a sampling calorimeter that constitutes the barrel part of the hadronic calorimetry in ATLAS. It uses iron as passive material and plastic scintillators as active layers. The mechanically distinct central barrel ($|\eta| < 1$) is divided in two partitions, Long Barrel A and Long Barrel C. There are also two extended barrel partitions, EBA and EBC that cover $0.8 < |\eta| < 1.7$. Each partition is segmented in equal azimuthal angle (ϕ) intervals into 64 modules. The modules are divided into cells, which are grouped radially in three layers. Two bundles of wavelength-shifting fibres associated with each cell guide the scintillation light from the exposed sides of the module to a pair of photomultiplier tubes. For each tile calorimeter channel, the pulse shape is given by seven digital samples spaced by 25 ns. The signal amplitude and phase can be parameterized enabling the amplitude, pedestal value and peak position in time to be extracted. The tile calorimeter operation in ATLAS is described in detail in [18]

3.4.1 β measurement in the tile calorimeter

The tile calorimeter time and β measurement is described in details in [5]. The time-of-flight and hence the velocity of a candidate can be deduced from time measurements in the tile calorimeter cells along its trajectory.

In this analysis we use tile calorimeter cells along the particle trajectory with measured energy deposition above 500 MeV. The resolution of time measurements improves with deposited energy from 2.7 ns for cells with 500 MeVof deposited energy to 1.7 ns for cells with 2 GeVof deposited energy.

4 LLP signature in ATLAS

Since the mass of the LLPs in this analysis is measured from its velocity and momentum, the most important characteristic of LLPs is its velocity. Unlike muons, heavy LLPs produced at the LHC could travel with velocity significantly lower than the speed of light. We distinguish between three velocity ranges:

1. $\beta <\sim 0.7$**:** The MS signals left by an LLP with velocity in this range may be associated with the next bunch crossing. In this case the LLP itself can not trigger as a muon and, unless the event is selected by another object, it will be lost. If the event is selected by another object, a dedicated reconstruction software described in section 7 can recover the LLP hits from the next bunch crossing, and the mass of the LLP can be measured from its velocity and momentum.

2. $\sim 0.7 < \beta <\sim 0.95$**:** An LLP with velocity in this range may arrive late to the MS but its signals will be associated with the correct bunch crossing. The mass of such LLP can be measured from its velocity and momentum.

3. $\beta >\sim 0.95$**:** The MS signals of an LLP with velocity in this range are similar to those of a muon. In particular, its mass can not be measured from its velocity and momentum.

This thesis describes searches for two distinct types of new particles; $\tilde{g}$ R-hadrons which include a colored LLP and non-colored sleptons. Signature related to the LLP type is described below.

4.1 Long lived slepton interaction with ATLAS

Heavy long lived slepton would interact in the the detector like a muon. It would leave ionization signals throughout all the detector from the ID to the MS including the calorimeters. Being a color singlet, it is not expected to produce hadronic showers. In addition, its high mass reduces its Bremsstrahlung radiation, and therefore, it is not expected to produce electro magnetic showers.

4.2 Long lived R-hadron interaction with ATLAS

The fraction of R-hadrons charged in the ID varies with the hadronization model [12]. The larger the $\tilde{g}$-ball fraction, the larger the fraction of R-hadrons neutral in the ID. In the analysis presented in this thesis, the fraction of $\tilde{g}$-ball is treated as a free parameter.

$\tilde{g}$ R-hadron may emerge as neutral states from the pp collision and become charged by strong interactions of the included light quarks with the detector material, arriving as charged particle at the MS. The fraction of R-hadrons charged in the MS depends on the R-hadrons scattering model. Three scattering models are currently considered: the first is described in [19], the second in [20] and the third in [21]. The so-called generic scattering model described in [19], results in the largest fraction of R-hadrons charged in the MS.

Since most of the energy of the R-hadron is carried by the heavy $\tilde{g}$ which almost does not interact with the detector material, R-hadrons are not expected to loose a lot of energy through hadronic interactions with the detector [22, 23].

5 Measurement strategy

This thesis presents a MS based search for LLPs. Only particles arriving as charged to the MS are considered candidates in this analysis. To account for the different signature of R-hadrons which include a colored LLP and non-colored sleptons two independent analyses where performed:

1. **Slepton search**: Motivated by non-colored LLPs, this analysis employs a *combined reconstruction* method which requires combined ID and MS tracks, and uses a combined fit to MDT, RPC and tile calorimeter hit times to estimate β. The momentum used in the mass measurement is obtained from the combined MS + ID track, using hits corrected for β.

2. **R-hadron search**: Motivated by colored LLPs, which may be neutral in the ID, this analysis employs an *MS-standalone reconstruction* method. The MS-standalone reconstruction does not require a track or hits in the ID, and combines the MDT segment fit, RPC and tile calorimeter hit times to estimate β. When an ID track is associated with the standalone candidate, its momentum is used in the mass reconstruction. Otherwise the reconstructed track or trigger track momentum measured in the MS is used. Using the combined ID + MS track results in poor momentum reconstruction, even when both sub-detectors have tracks, for any candidate for which the charge is different between ID and MS.

In both the slepton and R-hadrons searches the mass of the LLPs is estimated from the β and momentum measurements using the relation $m = p/\gamma\beta$. Therefore, in both these MS based searches, the background is composed of high p_T muons with mis-measured β.
The strategy of the two analyses is to optimize three factors that dominate the performance of the search:

1. **Resolution and tails of** β : improving the β resolution and reducing the tails of the β distribution improve the signal mass width and reduce the background in the signal region. The β resolution was optimized by performing a combined fit using estimations from different subdetectors. Different combination methods and different requirements on consistency between β measurements in different subdetectors were studied. Corrections to compensate for the current calibration conditions were applied.

2. **Background estimation**: an accurate estimation of the background shape and quantity is necessary in order to claim a discovery or set new limits. The background shape and quantity were estimated using only the data. Possible systematic uncertainties associated with the estimation method were studied.

3. **Signal significance**: different sets of background rejection cuts were considered. The sets of cuts in use are those that maximize the ratio between the expected number of LLPs and the expected number of background candidates, as obtained from the background estimation. Different cuts are used in the two analyses.

6 Data and simulated samples

The work presented in this thesis is based on 37 pb^{-1} of data collected by the ATLAS detector during 2010. In addition, 37 pb^{-1} of $Z \to \mu\mu$ enhanced events are used as a control sample. Background Monte Carlo (MC) samples in use are standard $Z \to \mu\mu$ samples. These samples are not used to study or estimate the background, but to correct the MC for the calibration condition observed in the data.

Signal MC samples are used to study the expected signal behavior and to set limits. All the samples were normalized to the integrated luminosity of the data, using cross-sections calculated to next to leading order, using the PROSPINO program [24]. The models, including the LLP mass and the production cross sections, are summarized in table 1.

The GMSB models were generated with $N_5 = 3$, $m_\mathrm{messenger} = 250$ TeV, sign$(\mu) = 1$ and tan$\beta = 5$. Their Λ values vary from 30 to 50 TeVand the corresponding $\tilde{\tau}$ masses from 101.9 to 160.7 GeV. The mass spectra were generated by the SPICE program [25]. The events were generated by

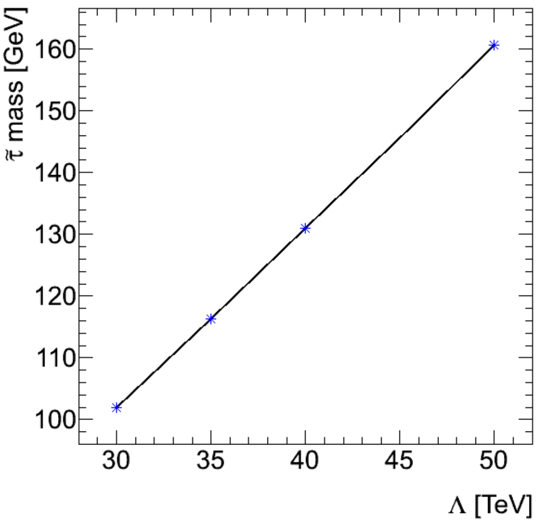

Figure 3: The slepton masses as a function of the GMSB parameter Λ. The other parameters are $N_5 = 3$, $m_{\text{messenger}} = 250$ TeV, sign(μ) = 1 and tan$\beta = 5$.

Herwig [26] and events passed full detector simulation [27, 28]. Figure 3 shows the slepton masses as a function of the GMSB parameter Λ.

In these models, the production can be strong, creating squarks in the hard interactions, which then decay via long chains ending finally in the NLSP, or there may be electroweak production where gauginos are produced first. The fraction of each type depends on the squark masses. The main production channels for the light $\tilde{\tau}$ are $\chi^0 \to \tilde{\tau}\tau$. The χ^0 can either decay directly to a $\tilde{\tau}$, or it can decay to a another slepton ($\tilde{\mu}$ or $\tilde{e}$) that later decays to a $\tilde{\tau}$. Due to R-parity and lepton number conservation, the decay products of the $\tilde{\mu}$ ($\tilde{e}$) are a $\tilde{\tau}$, a muon (electron) and a tau. The weak coupling to the gravitino LSP dictates the existence of two long-lived sleptons in each event. Their β spectrum covers large range with tendency towards high β values. Figure 4 shows the β (left) and p_{T} (right) distributions in the different GMSB samples we used. The β spectra of the sleptons produced in electroweak processes are shown in Figure 5.

Pair production of $\tilde{g}\tilde{g}$ was simulated in Pythia [29], incorporating specialized hadronization routines [30] to produce final states containing R-hadrons. The simulation of R-hadron interactions in matter is handled by dedicated Geant4 routines based on three different models with alternative assumptions. In the samples presented in detail in this note, the scattering model used to describe the $\tilde{g}$ R-hadron interactions with the detector material is the generic model [19] and a 0.1 $\tilde{g}$-ball fraction is used. Figure 6 shows the β (left) and p_{T} (right) distributions of some of the R-hadron

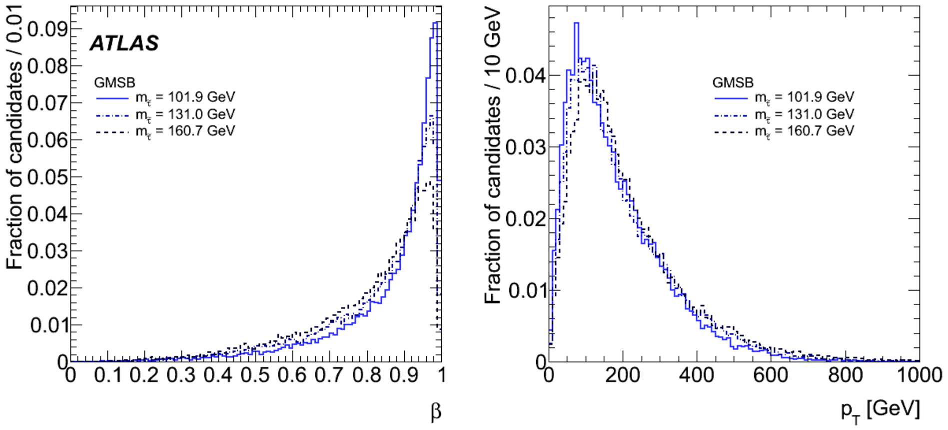

Figure 4: The slepton β (left) and p_{T} (right) distributions in the different GMSB samples.

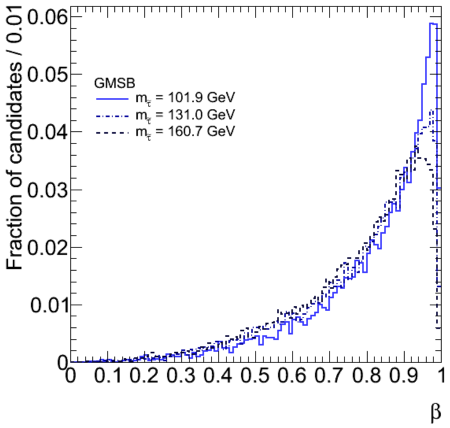

Figure 5: The β distribution of the sleptons produced in electroweak processes in the different GMSB samples.

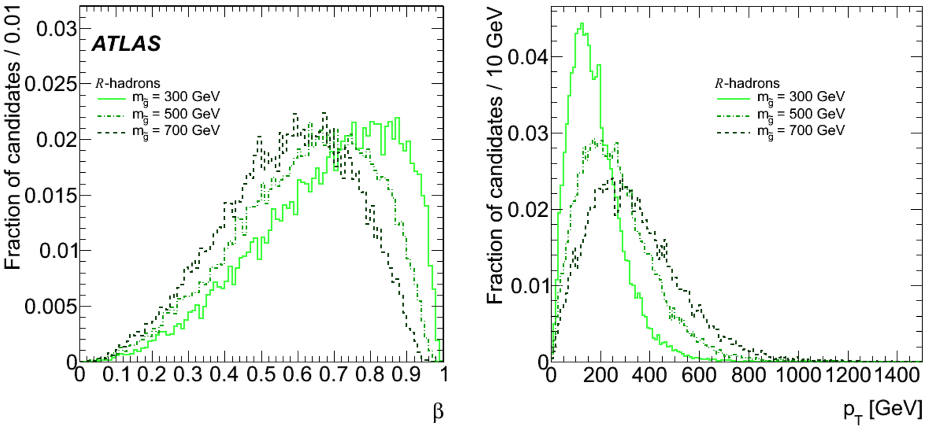

Figure 6: The R-hadron β (left) and $p_{\rm T}$ (right) distributions in the different R-hadron samples.

samples.

For completeness, different scattering models [20, 21] and different $\tilde{g}$-ball fractions (0.5 and 1.0) were also studied. These models were generated for $\tilde{g}$'s with masses 300, 500 and 700 GeV.

Model	LLP	LLP mass [GeV]	cross section [pb]
GMSB $\Lambda = 30$	$\tilde{\tau}$	101.9	2.388
GMSB $\Lambda = 35$	$\tilde{\tau}$	116.3	0.936
GMSB $\Lambda = 40$	$\tilde{\tau}$	131.0	0.454
GMSB $\Lambda = 50$	$\tilde{\tau}$	160.7	0.109
Split SUSY	$\tilde{g}$	300	62.1
Split SUSY	$\tilde{g}$	400	10.4
Split SUSY	$\tilde{g}$	500	2.34
Split SUSY	$\tilde{g}$	600	0.634
Split SUSY	$\tilde{g}$	700	0.194

Table 1: Signal MC samples: The GMSB models were generated with $N_5 = 3$, $m_{messenger} = 250$ TeV, sign$(\mu) = 1$ and tan$\beta = 5$. They differ by their Λ value. The generic model is used to determine the R-hadrons scattering.

7 Reconstruction of Long-Lived Charged Particle Candidates

Standard muon reconstruction efficiency starts dropping sharply for particles with $\beta < 0.75$ and is zero for particles with $\beta = 0.4$. This is due to two main issues: the data may not be associated with the event if the particle's hits are in the next bunch crossing; late arrival of the particle spoils segment fitting in the MDTs. We reconstruct slow particles and estimate their velocity and mass with a muon identification package [31] which is less sensitive to these effects.

7.1 The combined (MS+ID) reconstruction method

in the slepton search, we use a muon identification package (MuGirl) [31] which is efficient in identifying candidates even when the segment reconstruction is imperfect. This algorithm extrapolates ID tracks into the MS stations, searches for MS hits in a road around the extrapolated track and combines them into segments. As segments are found, further extrapolation starts from them, enabling the reduction of road sizes. Once all hits and segments along the track are found, an artificial neural network is used to decide if the features in the MS indicate a muon (or LLP). Finally, a track fit is performed combining ID and MS hits. The performance of this method for muons is similar to that of other combined muon algorithms in terms of efficiency, fake rates and momentum resolution, with a better efficiency in regions where the MS coverage is less complete.

The slow particle reconstruction is based on the following techniques: recovering trigger detector hits from the next bunch crossing, estimating the particle velocity from the RPC, tile calorimeter and MDT hits time or selecting the β that minimizes the MDT segments χ^2. The search in the MDT starts with the full set of hits found in the road around the extrapolated track, rather then the hits associated with the segment, so that extra hits that have been missed by the segment fit with $\beta = 1$ can be associated with a segment under a different β hypothesis. Candidates which fail identification as muons but are reconstructed as LLPs are kept, and they are used later in the analysis. From the estimated velocity and momentum of each candidate we estimate it's mass.

The reconstruction methods are described in detail in [32], some improvements have been introduced, including the addition of a track refit after β has been determined. Refitting the track at this point results in a better momentum resolution since it has the advantage of using a set of hits which were corrected to take into account the late arrival of the LLP to the different sub-detectors. Figure 7 shows the combined ID+MS reconstruction efficiency of LLPs as a function of β, p_{T}, η and ϕ. The efficiency is calculated for sleptons with $p_{\mathrm{T}} > 20$ GeVand $|\eta| < 2.5$ as the ratio between

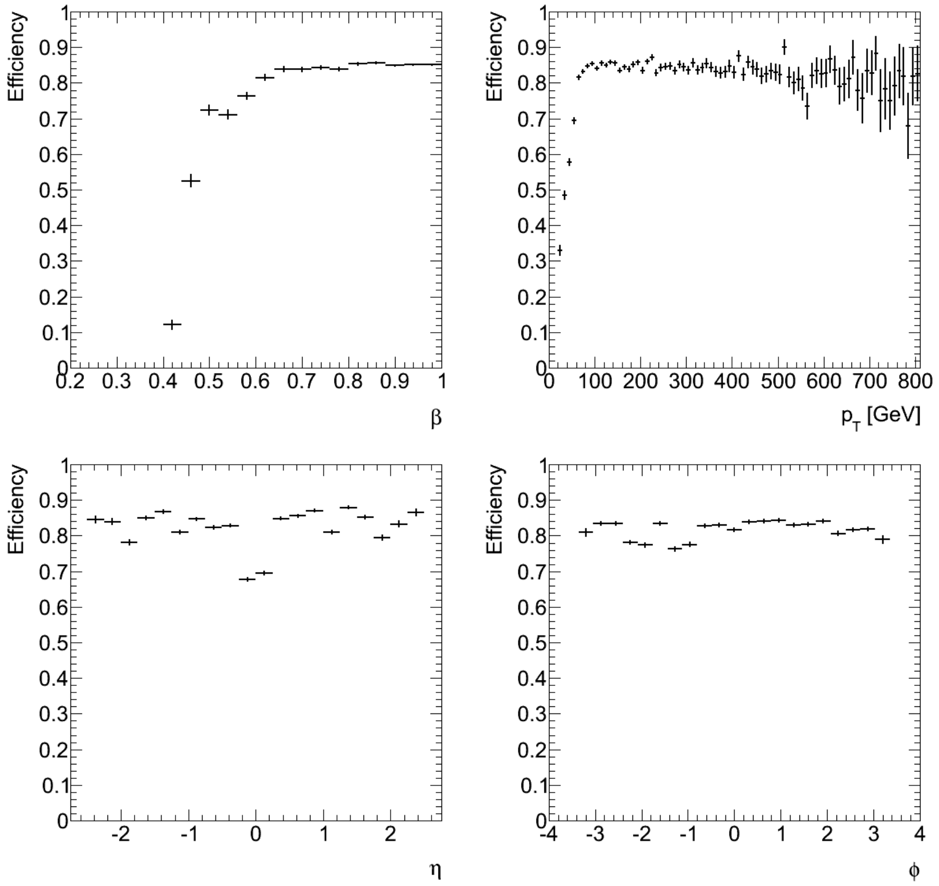

Figure 7: The combined ID+MS reconstruction efficiency of LLPs as a function of β, p_{T}, η and ϕ.

the number of the sleptons found by the combined reconstruction algorithm and the number of generated sleptons. No trigger selection is applied. We would like to emphasize that this reconstruction method is expected to be efficient for any LLP with a muon-like signature.

7.2 The MS-standalone reconstruction method

In the R-hadron search, in order to recover candidates which are neutral in ID, we employ a method that only relies on the MS. A different branch of MuGirl is used for LLP reconstruction, which is not used for muons. The reconstruction is seeded by a feature found by the muon event filter [15], without requiring a match with the ID. This branch of the reconstruction collects hits and segments starting from the position and momentum of the event filter candidate in the middle station of the MS and extrapolates the track to the inner and outer stations. Finally, once all segments are recon-

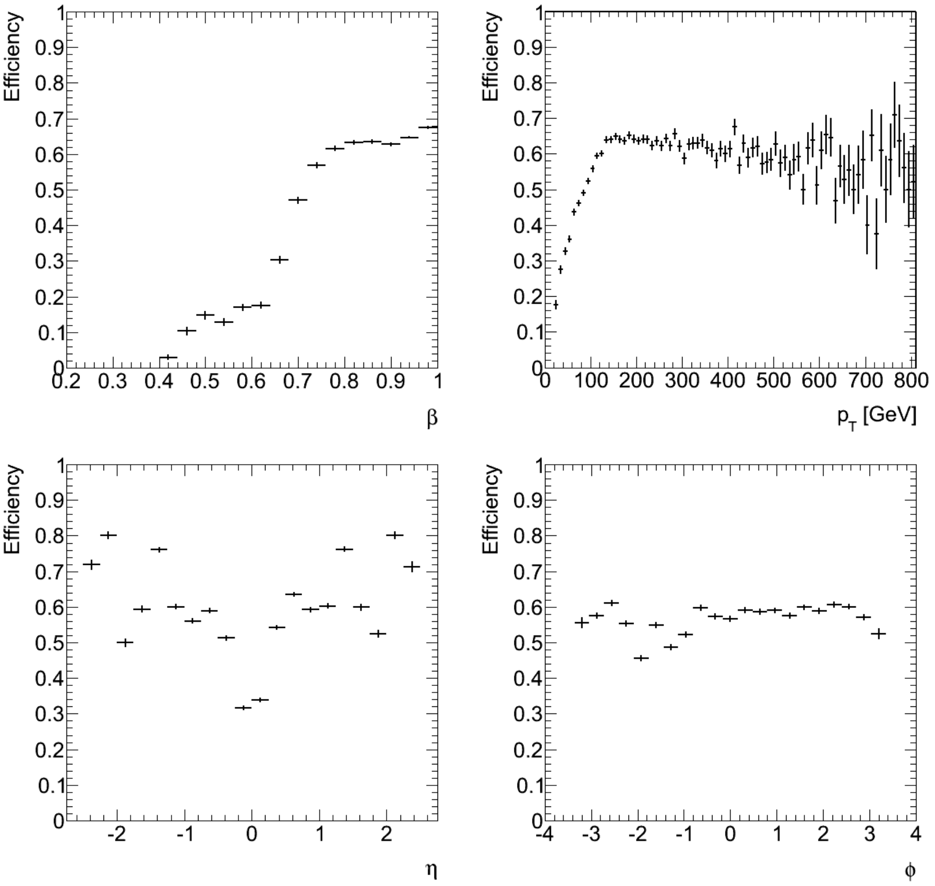

Figure 8: The MS-standalone reconstruction efficiency of LLPs as a function of β, p_{T}, η and ϕ.

structed, β is estimated. A candidate which is not found by the muon event filter, i.e. if it arrives late to the trigger chambers and its hits are not associated with the bunch crossing, is not reconstructed in the MS-standalone method. Figure 8 shows the MS-standalone reconstruction efficiency of LLPs as a function of β, p_{T}, η and ϕ. The efficiency is calculated for sleptons with $p_{\mathrm{T}} > 20$ GeVand $|\eta| < 2.5$ as the ratio between the number of the sleptons found by the MS-standalone reconstruction algorithm and the number of generated sleptons. No trigger selection is applied, but candidates are reconstructed only if found by the trigger. The large efficiency drop below $\beta = 0.6$ demonstrate the loss due to requiring an event filter feature as a seed.

8 Estimating β

We estimate β by minimizing the χ^2 between the set of available timing measurements and the timing expected from test βs, using the Golden Search minimization method [33]. The golden section search is a technique for finding the extremum (minimum or maximum) of a unimodal function by successively narrowing the range of values inside which the extremum is known to exist. The core of this method is a work function which is called with a β and returns the corresponding χ^2. According to the value of the χ^2, the minimization function determines the next β to process. The χ^2 is calculated for different technologies and techniques.

8.1 MDT segments

An MDT segment is reconstructed as a line tangent to the circles in the different layers, after the radii in the tubes were estimated from the drift time. The estimated drift time is $t_{\mathrm{measured}} - t_0$, and the radii, $R(t_{\mathrm{measured}} - t_0)$, but t_0 is based on particles passing the detector at the speed of light. Slow particles have a longer time-of-flight, and therefore, in order to obtain a good segment fit, t_0 must be computed from their arrival time to the detector. For each β in the minimization process, new MDT segments are built from a set of hits in a road around the extrapolated track, using a new t_0 corresponding to the arrival time of a particle traveling with the hypothesized β, $R(t_{\mathrm{measured}} - t_0(\beta))$. The minimization is to the χ^2 representing the difference between the measured position of the particle in the tubes and the segment position in the tube. For a low-β particle, this method recovers hits on segment that could be lost when fitting the segment with $\beta = 1$. χ^2 can only be minimized over a β range with equal number of hits on segments. This range is defined prior to the minimization process.

8.2 MDT hits

Once β was estimated with the method above, and a set of hits-on-track with the corresponding times of arrival are available, a full track fit is performed using the ID and MS hits. The estimated position where the track passed in each tube is significantly more accurate after the full track fit than in the segment finding stage. The time-of-flight of the particle to each tube is obtained using the difference between the time-of-flight corresponding to the refitted track position in the tube, t_{R} and the time actually measured, $t_0 = t_{\mathrm{measured}} - t_{\mathrm{R}}$. The error of the time measurement is estimated from the width of the chamber's t_0 distribution as explained in section 8.6, and the minimization is done with respect to the χ^2 between the measured time-of-flight and the time-of-flight corresponding to the arrival time of a particle traveling with the hypothesized β. This technique is suitable for the combined ID and MS reconstruction method.

8.3 RPC

The χ^2 corresponds to the difference between the measured time-of-flight and the time-of-flight corresponding to the arrival time of a particle traveling with the hypothesized β. The signal propagation time along the RPC strip is subtracted to obtain the measure time-of-flight. The measured time-of-flight is assigned an error which is estimated from the width of the distribution representing the difference between the measured muon time-of-flight and the expected muon time-of-flight as explained in section 8.6.

8.4 Tile

The tile calorimeter time measurement is described in [5]. The χ^2 corresponds the difference between the measured time-of-flight and the time-of-flight corresponding to the arrival time of a particle traveling with the hypothesized β. In [5] each time measurement is assigned an error according to the energy deposition such that cells with larger energy deposition have smaller error and bigger weight in the β estimation. A similar method was tested, using the measured time resolution as a function of energy to be the error in the fit. However there was no significant improvement in the combined β resolution with respect to using a global error for all tile calorimeter cells. This could be because candidates selected in the MS have few tile calorimeter cells associated per candidate compared to the number of MS measurements.

The β distributions in the data are different for candidates in the slepton search and in the R-hadron search. In the slepton search, the distributions are shown for candidates with $p_{\mathrm{T}} > 30$ GeV. In the R-hadron search, the distribution are shown for candidates with $p_{\mathrm{T}} > 40$ GeV. In both searches, only candidates in the MS acceptance region, $|\eta| < 2.5$, from collision events with good primary vertex quality (as discussed in section 9.3) are included. Figure 9 shows the estimated β distribution from the MDT hits (left) and segments (right) for the slepton and R-hadron searches respectively. Figures 10, and 11 show the β estimation using RPC, and tile calorimeter respectively, for the set of hits found in the slepton (left) and R-hadron (right) searches. The detector coverage dominates the estimation efficiency, hence the large amount of entries in the MDT techniques compare to the RPC and tile calorimeter. The mean value and width of the β distribution in the different techniques are summarized in table 2. For the MDT and RPC the mean and width are of a gaussian fit between 0.9 and 1.1. For the tile calorimeter the mean and width are of a gaussian fit between 0.8 and 1.2. Note that tails and outliers in the lower β region are likely to yield a high

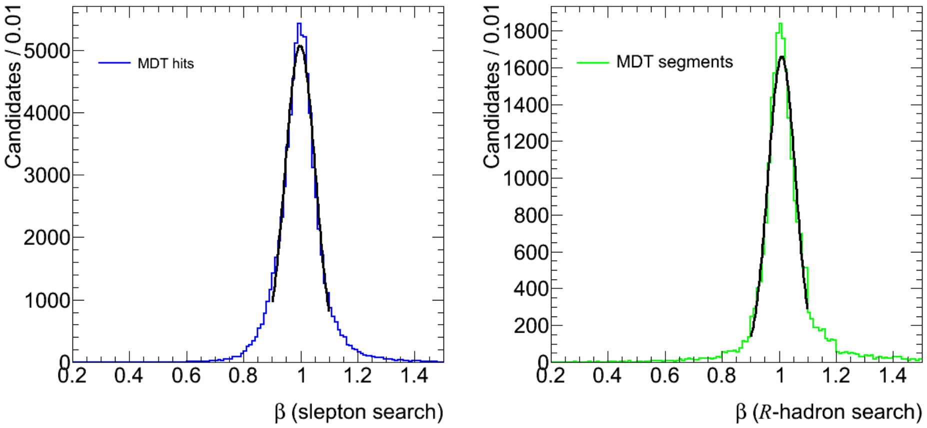

Figure 9: β measurement in the MDT. Left: candidates with $p_T > 30$ GeVin the slepton search using the MDT hits method. Right: candidates with $p_T > 40$ GeVin the R-hadron search using the MDT segments method. Only candidates with $|\eta| < 2.5$ from collision events with good primary vertex quality (section 9.3) are included. The β mean values are $\beta = 0.998$ and $\beta = 1.008$ and the resolutions are $\sigma = 0.053$ and $\sigma = 0.048$ for the slepton and R-hadron searches respectively.

mass measurement.

Technique	Slepton search		R-hadron search	
	mean β	σ_β	mean β	σ_β
MDT segments	-	-	1.008	0.048
MDT hits	0.998	0.053	-	-
RPC	0.989	0.068	0.991	0.066
Tile calorimeter	1.006	0.104	1.005	0.108

Table 2: β resolution in the different techniques. For the MDT and RPC the mean and width are of a gaussian fit between 0.9 and 1.1. For the tile calorimeter, the mean and width are of a gaussian fit between 0.8 and 1.2.

8.5 Combined minimization

In the combined minimization, for every hypothesized β, the χ^2's of all technologies are summed to a single χ^2. In absence of a contribution of one of the techniques (in particular, in regions outside the acceptance of RPC and tile calorimeter), only available technologies are combined. Figure 12 shows the combined β distribution of sleptons candidate measured in the combined minimization using the MDT hits + RPC (blue) and using

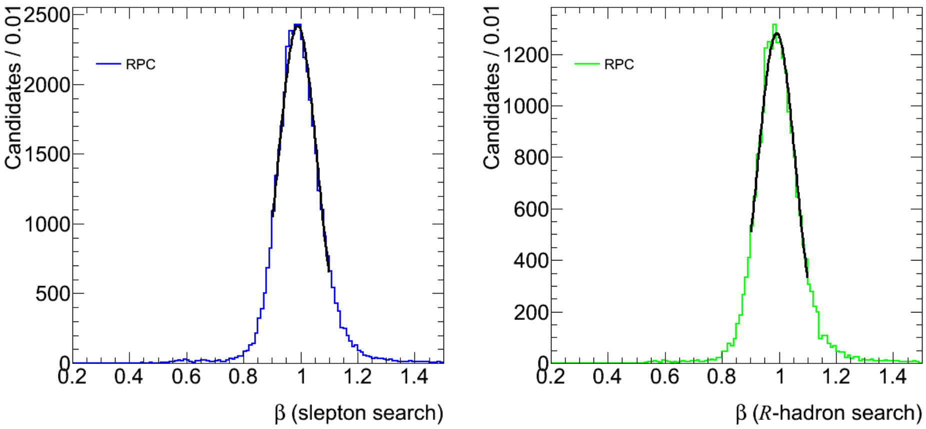

Figure 10: β measurement in the RPC. Left: candidates with $p_{\mathrm{T}} > 30$ GeV in the slepton search. Right: candidates with $p_{\mathrm{T}} > 40$ GeV in the R-hadron search. Only candidates with $|\eta| < 2.5$ from collision events with good primary vertex quality (section 9.3) are included. The β mean values are $\beta = 0.989$ and $\beta = 0.991$ and the resolutions are $\sigma = 0.068$ and $\sigma = 0.066$ for the slepton and R-hadron searches respectively.

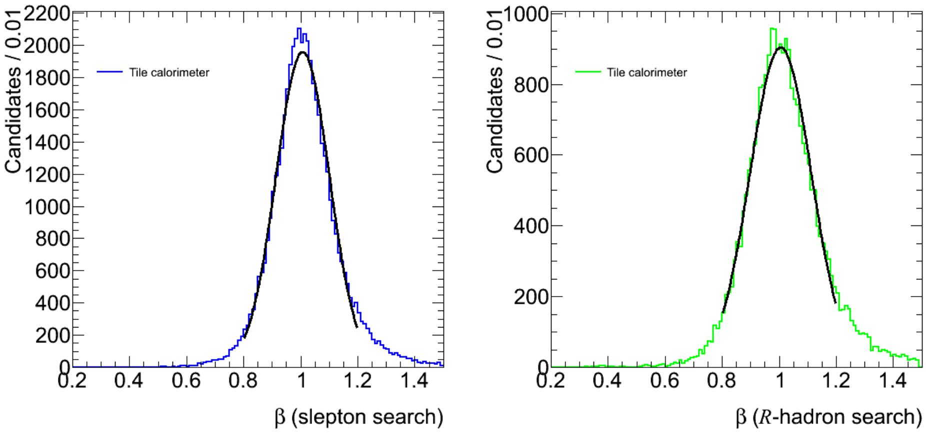

Figure 11: β measurement in the tile calorimeter. Left: candidates with $p_{\mathrm{T}} > 30$ GeV in the slepton search. Right: candidates with $p_{\mathrm{T}} > 40$ GeV in the R-hadron search. Only candidates with $|\eta| < 2.5$ from collision events with good primary vertex quality (section 9.3) are included. The mean values are $\beta = 1.004$ and $\beta = 0.998$ and the resolutions are $\sigma = 0.084$ and $\sigma = 0.098$ for the slepton and R-hadron searches respectively.

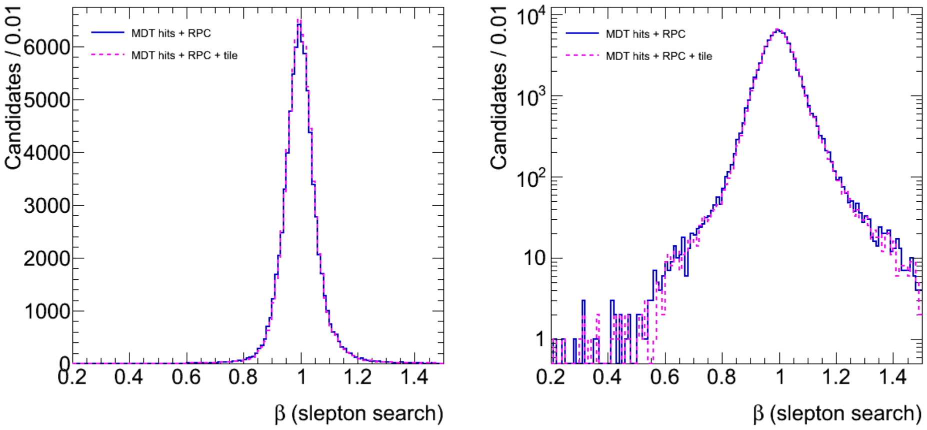

Figure 12: β measurement in the combined MDT hits+RPC (blue) MDT hits+RPC+tile calorimeter (magenta) minimization method, both in linear (left) and log (right) scales, of a set of hits found in the ID+MS reconstruction method. Only candidates with $p_{\mathrm{T}} > 30$ GeV and $|\eta| < 2.5$ from collision events with good primary vertex quality (more than 2 tracks and $|z_0| < 150$ mm) are included. The mean values are $\beta = 0.996$ and $\beta = 0.997$ and the resolutions are $\sigma = 0.049$ and $\sigma = 0.048$ respectively.

the MDT hits+RPC+tile calorimeter (magenta), both in linear (left) and log (right) scales. The mean values are $\beta = 0.996$ and $\beta = 0.997$ and the resolutions are $\sigma = 0.049$ and $\sigma = 0.048$ respectively. Although the β resolutions are similar, the tile calorimeter contributes a small improvements in the reconstruction efficiency and reduces the tails and outliers (the fraction with $\beta < 0.8$ is reduced from 0.73% to 0.66%). The combined MDT hits+RPC+tile calorimeter is the β estimation used in the slepton search.

Due to the lower quality of the tracking in the MS-standalone reconstruction, the MDT hits technique is less accurate in absence of combined MS+ID track. Therefore, in the R-hadronsearch the combined minimization is performed with the MDT segments. Figure 13 shows the β distribution of R-hadrons candidates measured in the combined minimization using the MDT segments+RPC (light green) and using the MDT segments+RPC+tile calorimeter (dark green), both in linear (left) and log (right) scales. The mean values are $\beta = 0.999$ and $\beta = 1.001$ and the resolutions are $\sigma = 0.053$ and $\sigma = 0.051$ respectively. The tile calorimeter contribution to the tail and outliers reduction is more significant here and the fraction with $\beta < 0.8$ is reduced from 1.9% to 0.8% when including the tile calorimeter. The combined MDT+RPC+tile calorimeter is the β estimation used in the R-hadron search.

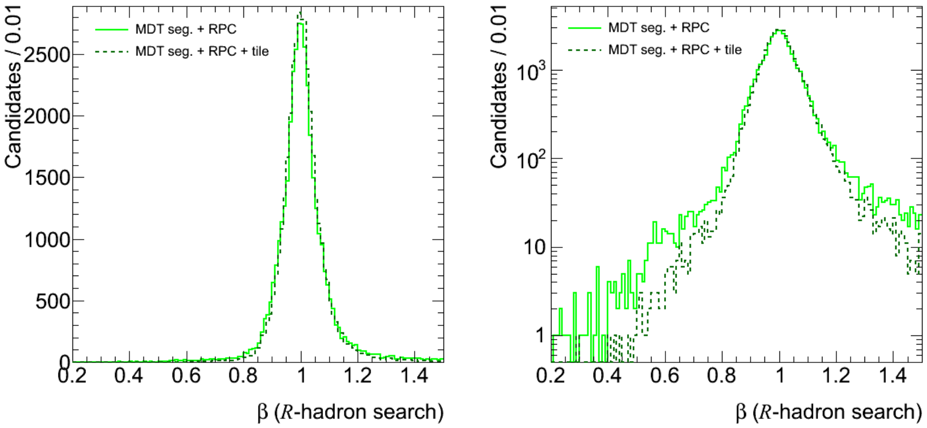

Figure 13: β measurement in the combined MDT segments+RPC (light green) MDT segments+RPC+tile calorimeter (dark green) minimization method, both in linear (left) and log (right) scales, of a set of hits found with the MS-standalone reconstruction method. Only candidates with $p_T > 40$ GeV and $|\eta| < 2.5$ from collision events with good primary vertex quality (more than 2 tracks and $|z_0| < 150$ mm) are included. The mean values are $\beta = 0.999$ and $\beta = 1.001$ and the resolutions are $\sigma = 0.053$ and $\sigma = 0.051$ respectively.

8.6 Calibration

The time-of-flight measurement is sensitive to the time resolution of the detector. The spatial resolution of the MDT, the RPC trigger efficiency and the energy resolution of the tile calorimeter are all affected by their time measurement resolution. Hence, the time calibration is an ongoing effort of the ATLAS collaboration and a big improvement has already been observed since the first data was collected. Nevertheless, the current time resolution of the different sub-detectors is not optimal yet, and is different from the resolution used in the MC. In ATLAS, the term t_0 represents the difference between the measured time-of-flight and the real time-of-flight of a particle from the interaction point to a detector element. In a well calibrated detector, t_0 in all the chambers should be distributed narrowly around 0. In 2010 this was not the case, and the t_0 distribution did not center at 0. Moreover, the distributions were different in different chambers. We applied a t_0 calibration and shifted the measured time-of-flight according to the shift of the t_0 distribution.

8.6.1 MDT calibration

In a perfectly calibrated MDT, any muon coming from a collision in the Interaction point will pass the detector at $t_0 = 0$. In 2010, a t_0 fit was performed as part of the segment making algorithm, to allow efficient muon reconstruction with initial MDT calibration condition. The t_0 distribution in the data was not centered at 0, and it was broader than in MC. The distribution was also different in different MDT chambers. We shifted the t_0 by chamber in the reconstruction software, and samples that were initially reconstructed with poor calibration have been reprocessed with better calibrations and their resolution improved.

8.6.2 RPC calibration

The RPC time measurement includes the signal propagation along the chamber. When the propagation time is subtracted, a calibrated RPC will measure $t = 0$ on average for a muon coming from the interaction point. In data, this is not yet the situation and different shifts from $t = 0$ are observed in the different RPC stations. The shifts are also different between different periods of data taking, and this is taken into account by finding similar sets of runs and making a number of different set of calibration shifts accordingly.

8.7 Optimization of the β measurement

To compensate for the shifts in t_0 a calibration process is performed as part of the β measurement. First, β is estimated as part of the muon reconstruction, as explained in section 8, and the corresponding hits are associated with the candidate. Then the hit times are shifted offline according to the observed mean of the corresponding t_0 distribution, in order to align the mean times of the distributions at $t = 0$. The observed widths of these distributions are used as an error on the time measurements, and the β fit is redone.

8.8 Muon β distribution in different η regions

The β distribution is different in different detector regions due to three main reasons:

1. Different η regions are covered by different technologies. In particular the acceptance of the RPC is in the range $0 < \eta < 1.05$, the acceptance of the tile calorimeter is in the range $0 < \eta < 1.7$ and the MDT covers the range $0 < \eta < 2.5$.

2. The accuracy of the time-of-flight method depends on the distance between the interaction point and the measurement point. The β measurement is more accurate when the distance between the interaction point and the detector element is larger.

3. The measurement in some regions of the detector is less accurate than in others. This is caused by in-homogenous magnetic field in some of

Region name	η	Slepton search		R-hadron search	
		mean β	σ_β	mean β	σ_β
BARREL1	$0 < \lvert\eta\rvert < 0.4$	0.983	0.057	0.998	0.061
BARREL2	$0.4 < \lvert\eta\rvert < 0.65$	0.991	0.062	0.996	0.068
BARREL3	$0.65 < \lvert\eta\rvert < 1.05$	0.987	0.045	1.006	0.055
ENDCAP1	$1.05 < \lvert\eta\rvert < 1.19$	0.997	0.053	1.011	0.052
ENDCAP2	$1.19 < \lvert\eta\rvert < 1.4$	1.004	0.049	1.002	0.063
ENDCAP3	$1.4 < \lvert\eta\rvert < 1.7$	1.007	0.042	1.011	0.048
ENDCAP4	$1.7 < \lvert\eta\rvert < 2.0$	1.008	0.036	1.003	0.031
ENDCAP5	$2.0 < \lvert\eta\rvert < 2.5$	1.007	0.036	1.000	0.026

Table 3: β resolution in the different η regions.

the regions. The measurement of the MDT may also be inaccurate if the particle track is in the same side of the wire in all the tubes.

The η regions and the β resolution in each region are summarized in table 3. The corresponding β distributions are shown in figures 14 and 15 for the slepton and R-hadron searches respectively. In the forward regions (ENDCAP4 and ENDCAP5) where the ID tracking is less accurate, the method using MDT hits, which relies on the combined track, performs worse than the method based on MDT segments.

9 Expected number of LLPs

The ability to discover or set a new limit on the mass of LLPs, depends on the expected number of LLPs in the data. This number varies between the different models and is sensitive to the expected signal resolution, the detector acceptance and the efficiency of the selection.

9.1 Signal resolution expected in data

The signal mass resolution in the MC is better than expected in the data, since in the MC the detector is assumed to be well calibrated. However, estimating the expected signal efficiency requires understanding of how a signal would look in the data in its current state. This is done by smearing of the hit times in the MC to reproduce the widths of the sub-detector time distributions observed in data. Figure 16 shows the muon β distribution of muons from the decay $Z \to \mu\mu$ in data (black) and smeared MC. The distributions are shown for muons in the slepton (left) and R-hadron (right) searches. It can be seen that the smearing mechanism reproduces the measured muon β distribution in the MC. Systematic uncertainties associated with the smearing mechanism are discussed in section 11. Once the time

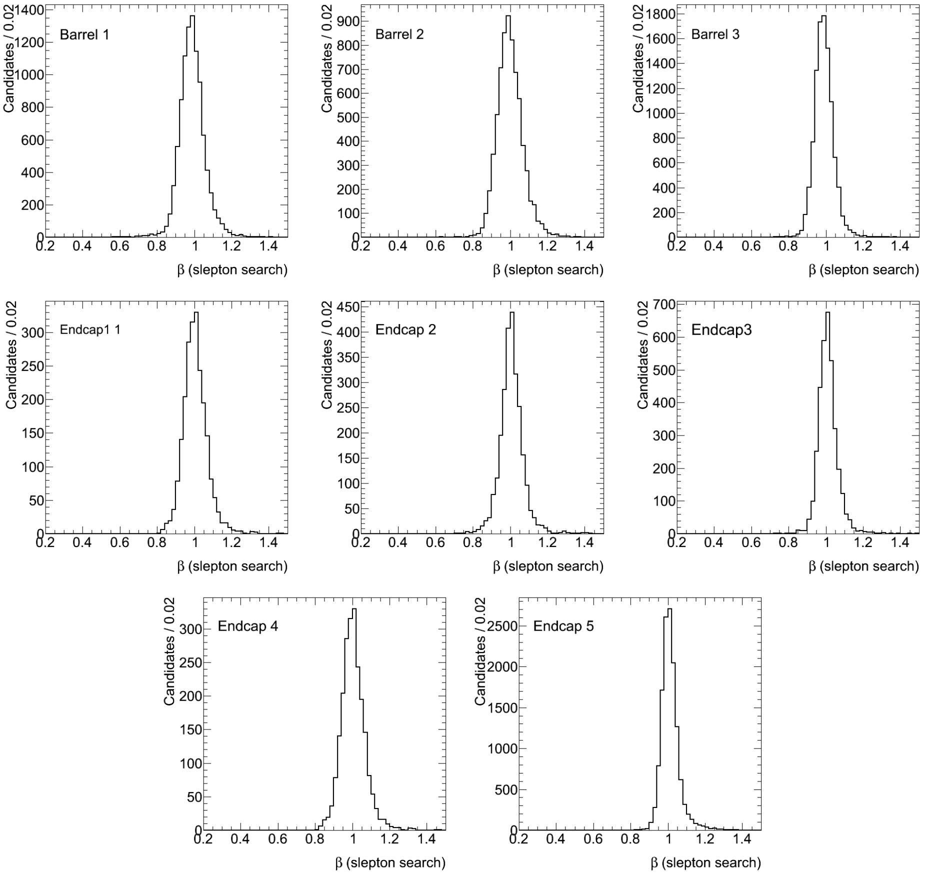

Figure 14: Distributions of β in the different η regions for the MS+ID combined reconstruction method. Only candidates with $p_\mathrm{T} > 30$ GeV and $|\eta| < 2.5$ from collision events with good primary vertex quality (more than 2 tracks and $|z_0| < 150$ mm) are included. The resolutions in the different regions are summarized in table 3.

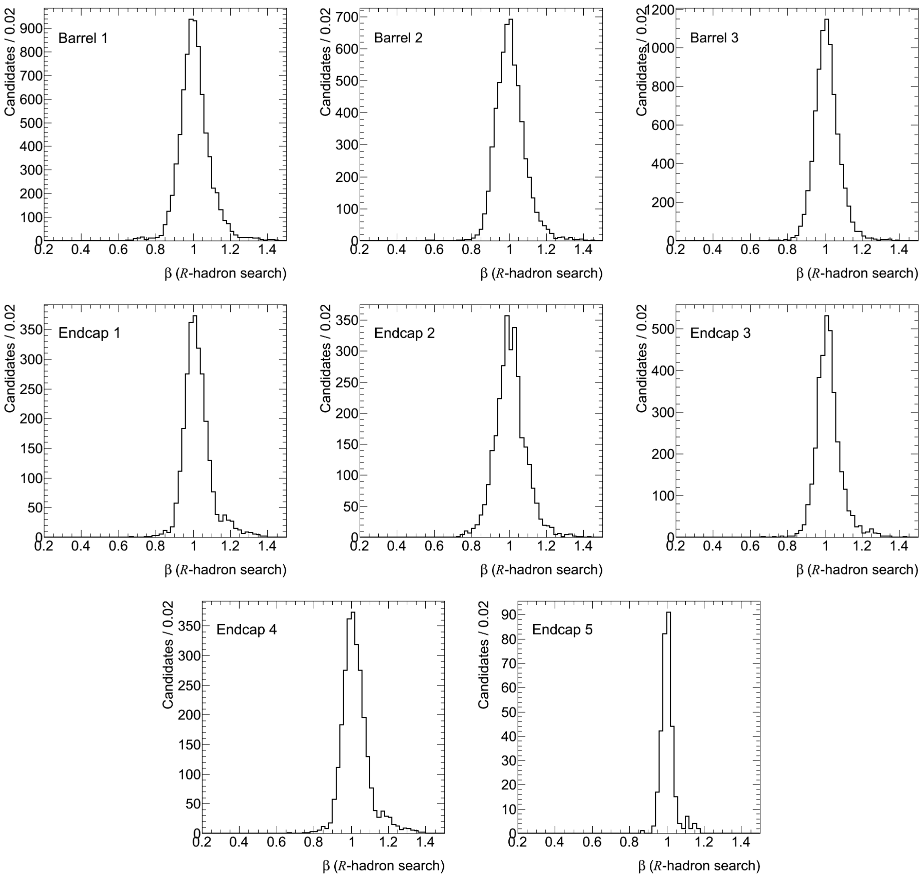

Figure 15: Distributions of β in the different η regions for the MS-standalone reconstruction method. Only candidates with $p_{\mathrm{T}} > 40$ GeV and $|\eta| < 2.5$ from collision events with good primary vertex quality (more than 2 tracks and $|z_0| < 150$ mm) are included. The resolutions in the different regions are summarized in table 3.

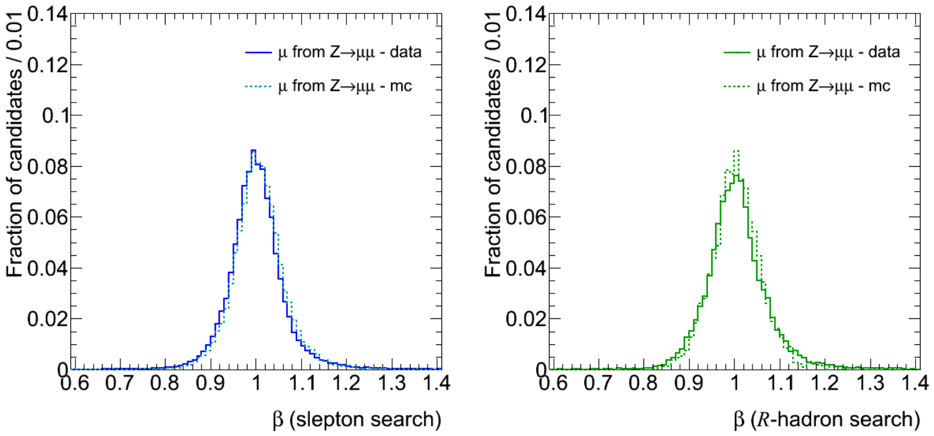

Figure 16: muon β distribution of muons from the decay $Z \to \mu\mu$ in data (black) and smeared MC, in the combined reconstruction method (left) and MS-standalone reconstruction method (right). Candidates in these plots passed the primary vertex, cosmic veto, candidate quality and β quality selection criteria discussed in section 9.3. The p_{T} cuts were reduced to 30 GeV and 40 GeV for the combined and MS-standalone analyses respectively.

resolutions in the MC reproduce correctly those of the data, the β estimation would give the correct resolutions for signal β. It is expected that for a given time resolution, β resolution is better for low β since t is larger and $\sigma(t)/t$ smaller, but the MC is used to model this effect.

The simulation of the detector alignment and of the magnetic field could be slightly different than the real alignment and magnetic field. As a result, the momentum resolution in the MC is different than its resolution in the data. In order to account for this effect, the candidate momenta were smeared using standard ATLAS tools, assigning momentum smearing factors as a function of p_{T} and η. The effect of this smearing on the expected number of LLPs was negligible and a systematic error is assigned in section 11.

The resulting signal mass distributions are shown in Figure 17 for sleptons in GMSB models in the slepton search (left) and for R-hadrons in the R-hadron search (right). The second peak at half the R-hadron mass is due to R-hadrons with 2 units of charge which, as a result, are reconstructed with half their true momentum. Table 4 summarizes the signal mass resolution expected in the data. For the $\tilde{g}$ R-hadrons the numbers describe the main peak.

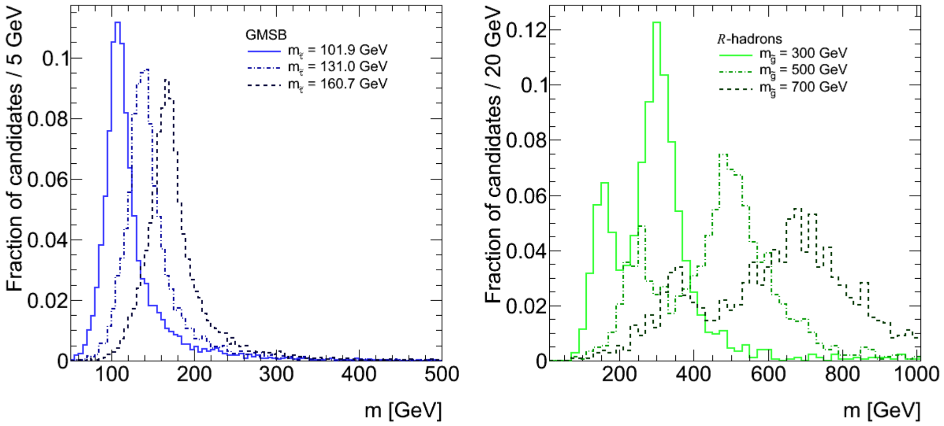

Figure 17: Expected LLP mass distributions. Left: sleptons in GMSB models reconstruction in the slepton search. Right: $\tilde{g}$ R-hadrons reconstruction in the R-hadron search. Candidates in these plots passed the selection criteria discussed in section 9.3.

Model	$M_{generated}$ [GeV]	$M_{measured}$ [GeV]	σ_M [GeV]
GMSB30	101.9	104.0	15.2
GMSB35	116.3	122.6	14.6
GMSB40	131.0	137.3	17.9
GMSB50	160.7	166.01	19.1
Split SUSY	300	302.2	30.2
Split SUSY	400	404.9	52.0
Split SUSY	500	498.9	55.4
Split SUSY	600	604.4	72.0
Split SUSY	700	692.2	88.3

Table 4: Expected signal mass resolution. The numbers of the $\tilde{g}$ R-hadrons describe the main peak.

9.2 Trigger selection

This analysis presented in this thesis is based on events collected by two types of muon trigger chains. The trigger for the slepton search requires MS tracks to be matched with ID tracks in the high-level trigger. The estimated p_{T} is obtained from the combination of both systems, and is required to satisfy $p_{\mathrm{T}} > 13$ GeV. The trigger for the R-hadron search requires an MS-standalone muon trigger with $p_{\mathrm{T}} > 40$ GeV. The standalone triggers have less accurate p_{T} estimates than the combined ones.

The events are selected online by requiring at least one muon level-1 trigger. As level-1 muon triggers are accepted and passed to the high-level trigger only if assigned to the collision bunch crossing, late triggers due to late arrival of the particles are lost. The level-1 trigger efficiency for particles arriving late at the MS is difficult to assess from data, where the overwhelming majority of candidates are muons. This efficiency is obtained from simulated R-hadron and GMSB events passing the level-1 trigger simulation. The estimated trigger efficiencies for GMSB slepton candidates are between 80% and 81%. The R-hadron search is much more adversely affected by the loss of trigger efficiency for late candidates, since the reconstruction is seeded by the trigger, and so even if an event is triggered by another object, the candidate will be lost. For R-hadrons that could be reconstructed because they are charged in the MS, the trigger efficiencies range between 55% for $m_{\tilde{g}} = 300$ GeV to 38% for $m_{\tilde{g}} = 700$ GeV. The estimated trigger efficiency with respect to all R-hadrons produced in the scattering model of [19] varies from 25% for $m_{\tilde{g}} = 300$ GeV to 17% for $m_{\tilde{g}} = 700$ GeV. The effect of the trigger efficiencies can be seen in tables 6 and 7.

9.3 Offline selection

Different event and candidate selection cuts were studied. Table 5 lists the cuts used to reject background in the slepton and R-hadron searches. The resulting candidates yields at different stages are summarized in table 6 and table 7 for the signal and data in the slepton and R-hadron searches respectively.

Collision events are selected by requiring a good primary vertex with at least three ID tracks, and with $|z_0^{\mathrm{vtx}}| < 150$ mm (where z_0^{vtx} is the z coordinate of the reconstructed primary vertex).

Cosmic-ray background is rejected by removing tracks that do not pass close to the primary vertex in z. For candidates with an associated ID track, candidates with $|z_0^{\mathrm{trk}} - z_0^{\mathrm{vtx}}| > 10$ mm are removed, where z_0^{trk} is the z coordinate at the distance of closest approach of the track to the origin. If no ID track is associated with the candidate, then it is still rejected if $|z_0^{\mathrm{trk}} - z_0^{\mathrm{vtx}}| > 150$ mm. Pairs of candidates with approximately opposite η and ϕ are also removed.

The analysis searching for sleptons requires two candidates in each event, because two sleptons are produced, and both have a high probability to be observed in the MS. However, only one of them is required to pass the LLP selection. This requirement reduces background from W production and QCD, but $Z \rightarrow \mu\mu$ decays remain. Any candidate that combines with another muon to give an invariant mass within 10 GeV of the Z mass is rejected. In the R-hadron search, no requirement of two candidates per event is made, because R-hadrons may be neutral in the MS, or be lost by triggering in the next bunch crossing. Nevertheless, pairs consistent with the Z mass are still rejected in the R-hadron search. These requirements are grouped in tables 6 and 7 under the label "event selection".

The slepton search requires candidates to have $p_{\mathrm{T}} > 40$ GeV, well above the efficiency plateau for the trigger threshold of 13 GeV. A p_{T} requirement of 60 GeV is applied for all candidates in the R-hadron search, so as to be in the MS-standalone trigger-efficiency plateau. Candidates with $p_{\mathrm{T}} >$ 1 TeV are rejected. This removes a few candidates with badly reconstructed momenta in both searches. Each candidate is required to have $|\eta| < 2.5$. These requirements are grouped in tables 6 and 7 under the label "candidate quality".

The estimated β is required to be consistent for measurements in the same sub-detector, based on the RMS of β calculated from each hit separately. The estimated β is also required to be consistent between subdetectors. A β measurement in at least two subdetectors is required for $|\eta| < 1.7$. These requirements are grouped in tables 6 and 7 under the label "β quality". Finally, in order to reject muons, the combined β measurement is required to be in the range $\beta < 0.95$. For signal, a low β should be correlated between measurements whereas for muons they are a result of poor estimation and should be uncorrelated between measurements. If the candidate $|\eta| < 1.7$ two β measurements are required. Figure 18 shows p_{T} distribution in three η regions where sufficient statistics are available. Although it can be seen that the p_{T} distribution varies between the different η regions, the distributions before (red) and after (blue) applying the cut $\beta < 0.95$ are consistent.

9.4 Cosmic background contamination

Cosmic muons arrive at the detector in random times. Hence, cosmic muons associated with a collision bunch crossing, may fake low β candidates. We do not use timing cuts to reject cosmic rays in this analysis, since such cuts could reduce the signal efficiency. As mentioned in the previous section, cosmic rays are rejected with the requirement on $|trk_{z_0} - vtx_{z_0}|$ and by using a topological cut which rejects any 2 candidates with opposite η and ϕ ($|\eta_1 + \eta_2| < 0.005$, $||\phi_1 - \phi_2| - \pi| < 0.005$). The efficiency of these cuts to reject cosmic ray was tested on barrel data collected with a cosmic

		Slepton search	R-hadron search
Event	PV quality	$\vert z0\vert < 150$ mm > 2 tracks	$\vert z0\vert < 150$ mm > 2 tracks
	Cosmic veto	2 candidates with opposite η and ϕ $\vert trk_{z_0} - vtx_{z_0}\vert < 10$ mm	2 candidates with opposite η and ϕ $\vert trk_{z_0} - vtx_{z_0}\vert < 150$ mm or $\vert trk_{z_0} - vtx_{z_0}\vert < 10$ mm if ID
	$Z \rightarrow \mu\mu$ veto	80 GeV $< m_{\mu\mu} <$ 100 GeV	80 GeV $< m_{\mu\mu} <$ 100 GeV
	# candidates	>= 2	>= 1
CQ	p_{T}	40 GeV $< p_{\mathrm{T}} < 1TeV$	60 GeV $< p_{\mathrm{T}} <$ 1 TeV
	η range	$\vert\eta\vert < 2.5$	$\vert\eta\vert < 2.5$
β Q	β consistency	2 βs consistent within 5σ	2 βs consistent within 5σ
	β quality	RMS $< 3\sigma$	RMS $< 5\sigma$
	# technologies	$>$ 1 estimation if $\vert\eta\vert < 1.7$	$>$ 1 estimation if $\vert\eta\vert < 1.7$
	β range	$\beta < 0.95$	$\beta < 0.95$

Table 5: Selection cuts: event (including primary vertex, PV) , candidate quality (CQ), β quality (βQ) and β range.

		Λ [TeV] =	30	35	40	50
	data	$m_{\tilde{\tau}}$ [GeV] =	101.9	116.3	131.0	160.7
Before selection	-		146.4	61.7	28.7	7.3
Trigger selection	959921		119.1	50.4	23.3	6.5
Event selection	57382		107.0	45.6	21.4	6.0
Candidate quality	5134		91.4	38.8	18.3	5.2
β quality	3470		70.4	29.5	14.0	3.9
$\beta < 0.95$	582		51.8	21.7	11.2	3.0

Table 6: Candidates in data and simulated GMSB signal passing the selection stages in the slepton search. The Monte Carlo signal prediction is normalized to the data luminosity using the next to leading order cross-section.

	data	$m_{\tilde{g}}$ [GeV] =	300	400	500	600	700
Before selection	-		4542	761	177.7	46.4	14.2
Trigger selection	168043		1146	174	37.6	9.1	2.4
Event selection	150771		1140	173	37.4	9.0	2.4
Candidate quality	6334		504	75	15.7	3.8	1.0
β quality	4998		443	66	13.9	3.3	0.8
$\beta < 0.95$	830		420	64	13.5	3.2	0.8

Table 7: Candidates in data and simulated R-hadron signal passing the selection stages in the R-hadron search. The Monte Carlo signal prediction for the sample with the scattering model of [19] and a $\tilde{g}$-ball fraction of 0.1, is normalized to the data luminosity.

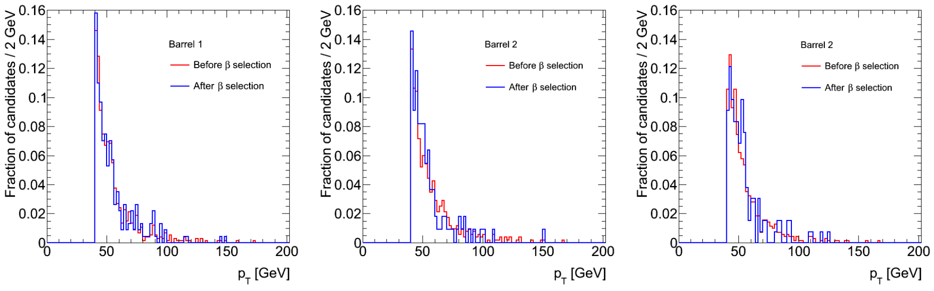

Figure 18: p_{T} distribution in three η regions where sufficient statistics are available

Λ [TeV]	$M\tilde{\tau}$ [GeV]	$M_{\tilde{\mu}} - M_{\tilde{\tau}}$ [GeV]	$\tilde{\mu}$ fraction [%]
30	101.9	1.91	27.7
35	116.3	1.97	30.5
40	131.0	2.06	0.4
50	160.7	2.3	0.4

Table 8: The $\tilde{\mu}$ fraction in the selected slepton sample before mass cut.

muon trigger in the empty bunches and periods without collisions, dropping the requirement of a good primary vertex. The cosmic veto rejected 98.0% ± 0.5% (699 of 713) of the cosmic rays for the standalone analyses and 76.1% ± 4.6% (67 of 88) for the combined analysis. We then run the analysis on collision events with and without the cosmic rejection, and calculate how many candidates are rejected by the cosmic rejection at each stage of the selection. From the number of rejected candidates and the rejection efficiency we estimate the remaining cosmics. The results of this calculation are that 1.3 ± 0.17 cosmic rays are left in our standalone sample after the $\beta < 0.95$ requirement. Of those 0.14, 0.08, 0.00 are estimated above the mass cuts 150 GeV, 250 GeV and 350 GeV respectively. The cosmic ray contamination in the combined analysis is 0.70 ± 0.17 candidates after the $\beta < 0.95$ requirement. Of those 0.36, 0.24, 0.20 are estimated above the mass cuts 90 GeV, 110 GeV and 130 GeV respectively.

9.5 Details of the slepton yields

If the mass difference between the light $\tilde{\mu}$ and the light $\tilde{\tau}$ is very small, the $\tilde{\mu}$ may also be long-lived. Table 8 shows the fraction of $\tilde{\mu}$ in the selected slepton sample before any mass cut.

Two stable sleptons are produced in each GMSB event. Table 9 shows the fraction of events that have two candidates with reconstructed mass above 90 GeV. The fraction is with respect to the number of events that have at least one candidate with reconstructed mass above 90 GeV. Table 6 above list the number of candidates passing the selection criteria. Table 11 below list the number of events passing the final selection. The limits in section 12 are obtained from the number of events in table 11.

10 Background estimation

The estimation of the background mass distribution is done directly from the data and does not use MC. It relies on two premises. That the signal to background ratio before applying cuts on β is very small, and that the probability density function (p.d.f.) for the β resolution for muons is

Λ [TeV]	$M\tilde{\tau}$ [GeV]	fraction [%]
30	101.9	22.3
35	116.3	25.8
40	131.0	28.6
50	160.7	32.4

Table 9: The fraction of events that have two candidates with reconstructed mass above 90 GeV.

independent of the source of the muon and its momentum.

The muon β p.d.f. in each η region (described in table 3) is the histogram of the measured β of all candidates in each region passing the selection criteria described in table 5, not including the selection $\beta < 0.95$. In order to enlarge the statistics, we omitted the requirements for more than one candidate and the Z veto. In addition, the p_{T} requirement in the slepton search was reduced to 30 GeV while in the R-hadron search the p_{T} requirement was kept at 40 GeV.

10.1 The background estimation method

We start from the full sample of candidates passing the selection criteria described in table 5, not including the selection $\beta < 0.95$. In this sample the $\imath$th candidate is reconstructed with momentum p_i and velocity β_i. We would like to emphasize that for a signal p_i and β_i are correlated via the mass of the new particle, while for a muon β_i may be different than 1 only due to the resolution of the β measurement. Therefore, if the full sample contains signal and background, than the histogram of the measured mass $m_i = p_i/(\gamma\beta)_i$ is expected to have a peak in the signal mass.

In order to obtain an estimate of the background reconstructed mass spectrum we use each candidate's measured momentum and ignore its measured β. Instead, for the $\imath$th candidate we draw a β from the β p.d.f. in the region. The $\imath$th candidate in our estimation has measured momentum p_i and fake β denote as β_j. If $\beta_j < 0.95$ the candidate is assigned a fake mass $m_j = p_i/(\gamma\beta)_j$. The statistical error of the background estimation is reduced by repeating the procedure 1000 times for each muon and dividing the resulting distribution by the number of repetitions. The histogram of mass obtained this way represents the background estimation. The procedure is done for in each η region separately, and only at the end, the background estimates from the different regions are added together.

For the muons, the measured β and the fake β are taken from the same distribution, therefore, the background is estimated correctly. For the signal, when drawing a β from the muon β p.d.f., the momentum and the β are no longer correlated. Most of the signal will get a β greater than 0.95 and will not enter the histogram of fake mass, and the remaining candidate's mass will be smeared over a large mass range due to the lack of correlation between their momentum and the fake β. Since the ratio of new particles to the muon background in the original candidate sample is small, the background distribution almost does not change in presence of the signal.

10.2 Muon β independence

The assertion that the β distribution is the same for all muons, whatever their kinematics is an important basis to the background estimation and requires careful checking.

10.2.1 Simulation studies

The study of the independence of the muon β p.d.f. in MC was performed at an early stage of the research. The combined MS+ID reconstruction method was used, and β was estimated from the combined MDT segments + RPC minimization. The study was performed prior to the decision to divide the detector into the eight regions defined in 3. Instead, the following four η regions were defined:

- The barrel, $\mid \eta \mid < 1.05$
- End-cap region 1, $1.05 <\mid \eta \mid < 1.5$ (excluding $1.2 <\mid \eta \mid < 1.35$)
- End-cap region 2, $1.5 <\mid \eta \mid < 2$
- End-cap region 3, $2 <\mid \eta \mid < 2.5$

We constructed the muon β p.d.f. in each η region from the histogram generated using the measured β of the following background sources:

- Muon pairs from Z decay ($Z \rightarrow \mu\mu$).
- Muons from W$\rightarrow\mu\nu$ decay.
- Muons from top decays.
- Muons from QCD processes.

Once the p.d.f. was available, we performed two statistical tests to ensure that the β distribution of any subset of muons is consistent with this p.d.f.. The tests we used were the Kolmogorov-Smirnov test, and a χ^2 test to verify that the ratio between the subset distribution and the muon β p.d.f. fits the zeroth order polynom $y = 1$. The subsets of muons we used were muons from the different background sources and muons in different momentum ranges.

The β measurement does not take into account the effect of bending in the magnetic field. For this reason, together with the effect of multiple scattering we expect that the β resolution of muons with low momentum will be slightly wider. To minimize these effects we demonstrated the muon β p.d.f. independence for muons with $p_T > 30$ GeV, consistent with the p_{T} selection requirements placed later in the data analysis.

Figure 19 shows the reconstructed β distributions of muons from Z decay (red), W decay (blue), top decays (green), and QCD (magenta) compared to the muon β p.d.f. (black) for the four η regions. The lower pad shows the ratio of the p.d.f. and the distribution of the subset. The Kolmogorov-Smirnov values distribute uniformly between 0 and 1, with no value significantly close to 0. We concluded that the Kolmogorov-Smirnov values gives no indication for differences between the β distributions of the muons from the different sources. The value obtained in a zeroth order polynomial fit of the ratio is consistent with expectations (14 times within 1 sigma from 1 and 2 times within 2 sigmas from 1). The χ^2 per degree of freedom shows good agreement between the ratio and the line $y = 1$.

Figure 20 shows the reconstructed β distributions of muons in the different momentum ranges. Due to the cut on the muon p_T, the momentum spectra is different in the different η regions. Therefore, in order to have enough statistics in the different ranges, we choose different momentum ranges in each η region. Table 10 summarizes the momentum ranges in the different η regions. The Kolmogorov-Smirnov values distribute uniformly between 0 and 1. We conclude that the Kolmogorov-Smirnov values gives no indication for differences between the β distributions of the muons in the different momentum ranges. The value obtained in a zeroth order polynomial fit of the ratio is consistent with expectations (11 times within 1 sigma from 1 and 1 time within 2 sigmas from 1). The χ^2 per degree of freedom shows good agreement between the ratio and the line $y = 1$.

Momentum range	low	medium	high
Barrel 1	$30 < p < 50$ GeV	$50 < p < 70$ GeV	$p > 70$ GeV
Endcap 1	$30 < p < 80$ GeV	$80 < p < 100$ GeV	$p > 100$ GeV
Endcap 2	$30 < p < 120$ GeV	$120 < p < 150$ GeV	$p > 150$ GeV
Endcap 3	$30 < p < 200$ GeV	$200 < p < 250$ GeV	$p > 250$ GeV

Table 10: Momentum ranges in the different η regions.

We conclude that in the simulation the β distribution does not depend on the source of the muon or its momentum.

10.2.2 Muon β independence in the data

The independence of the muon $]beta$ distribution was tested in data after they become available, with the limitation that the data are not conveniently

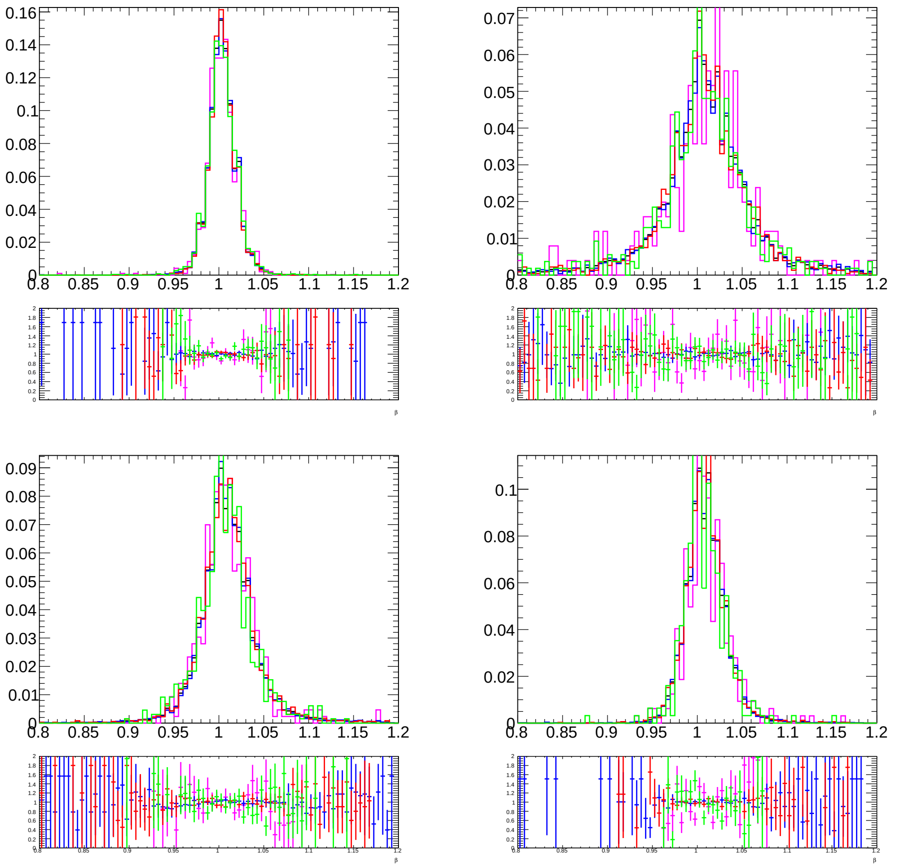

Figure 19: β distribution for muons from W+jets (blue), Z+jets (red), top events (green) and QCD (magenta) and the combined muon β p.d.f. (black) in the four η regions. In the lower pad is the ratio between the source β distribution and the muon β p.d.f..

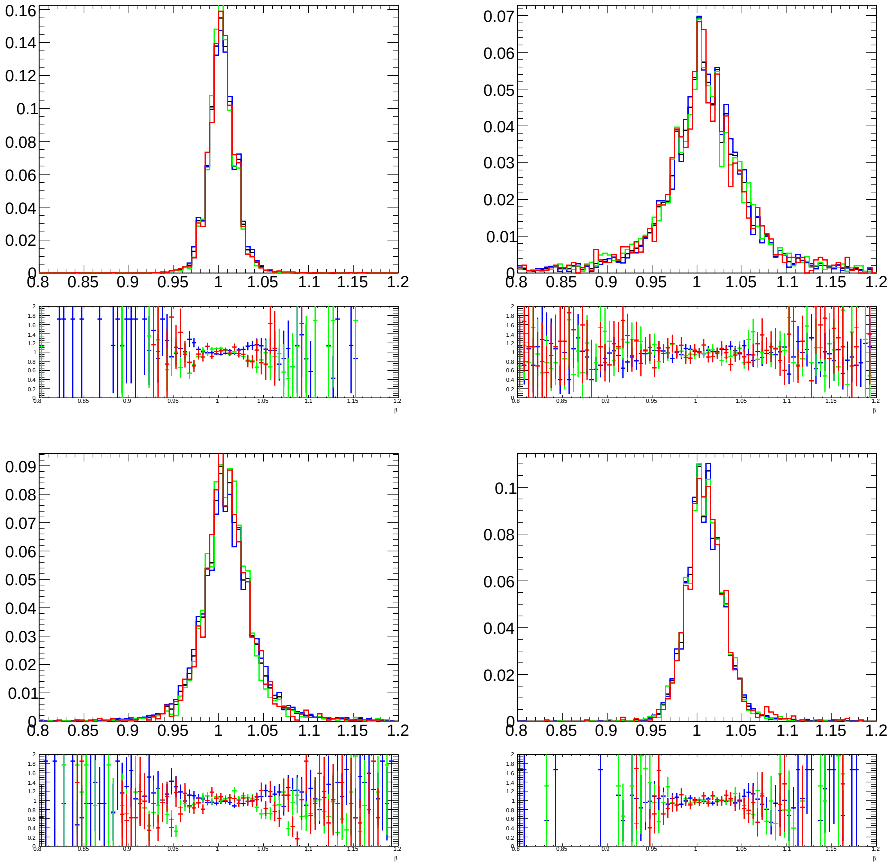

Figure 20: β distribution for muons from in different momentum ranges: low (blue), medium (green) and high (red), as defined in 10 and the combined muon β p.d.f. (black) in the four η regions. In the lower pad is the ratio between the momentum subset β distribution and the muon β p.d.f..

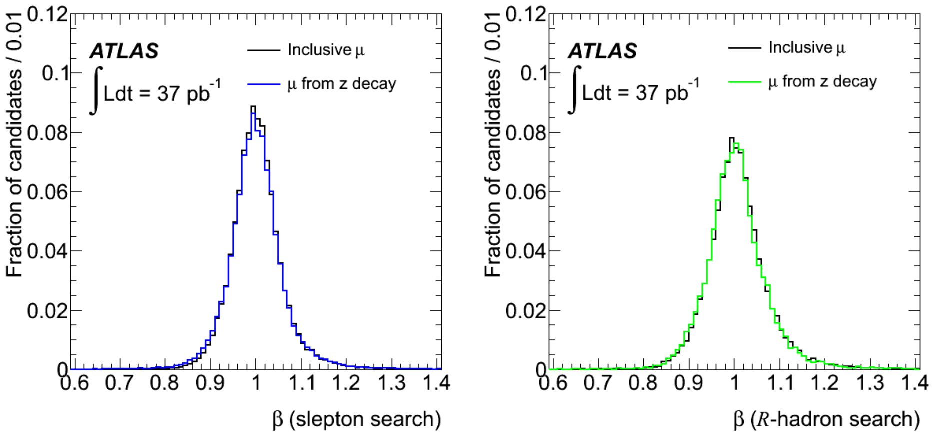

Figure 21: muon β distribution in data for inclusive candidates (black) and muons from $Z \rightarrow \mu\mu$ (color) in the combined reconstruction method (left) and MS-standalone reconstruction method (right). Candidates included in these plots passed the primary vertex, cosmic veto, candidate quality and β quality selection criteria discussed in section 9.3. The p_{T} cuts were reduced to 30 GeV and 40 GeV for the combined and MS-standalone analyses respectively. No source dependance of the muon β p.d.f. is observed.

divided by sources, except for Z decays which are relatively easy to identify.

Figure 21 shows the β distribution of all candidates in the data (black) and muons from $Z \rightarrow \mu\mu$ (color) passing the selection criteria presented in section 9.3, not including the requirement $\beta < 0.95$. The results are shown for the distribution obtained in the slepton search (left) and in the R-hadron search. It can be seen that the β p.d.f. is independent of the muon source.

To test the momentum dependence of the muon β p.d.f., in each η region, two β p.d.f.'s were obtained from the β measurement of candidates with high or low momentum only. The momentum thresholds separating high from low in each region were selected to provide enough candidates in both the high and low momentum ranges. Figure 22 shows that the difference between the resulting β p.d.f.'s is negligible for both slepton (left) and R-hadron(right) searches.

10.3 Estimated background

The reconstructed mass distribution in different regions of the detector depends on both β and momentum distributions through $m = p/\gamma\beta$. The regions also differ in the muon momentum distribution, since for any p_{T} cut, p is larger as η increases. Figures 23 and 24 shows the reconstructed mass and the estimated background mass distribution in the eight regions

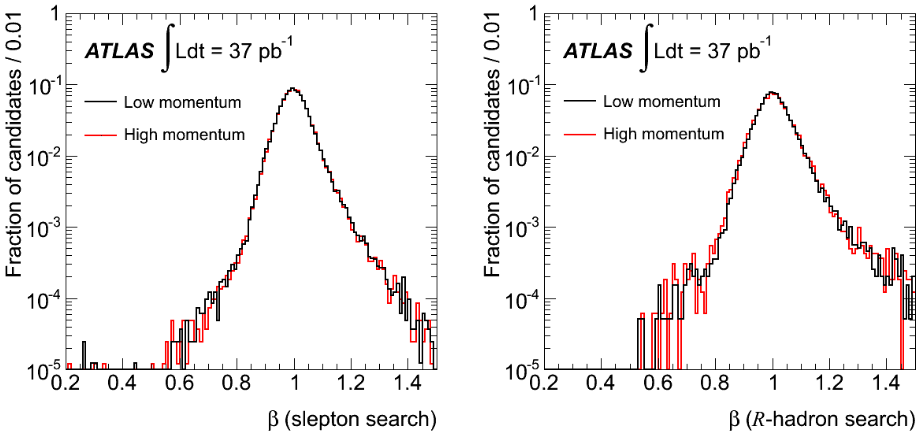

Figure 22: muon β p.d.f. obtained from muons with high (black) and low (red) momenta in the slepton search (left) and R-hadron search (right). Candidates included in these plots passed the primary vertex, cosmic veto, candidate quality and β quality selection criteria discussed in section 9.3. The p_{T} cuts were reduced to 30 GeV and 40 GeV for the slepton and R-hadronsearches respectively. No momentum dependance of the muon β p.d.f. is observed.

summarized in table 3 for the slepton and R-hadron searches respectively. The distributions are composed of candidates passing the selection criteria described in section 9.3.

The sum of the estimated background in all regions is shown in figure 25 for the slepton (left) and R-hadron (right) searches. The full mass range is shown in log scale (top) and the high mass region is shown in linear scale (bottom). It can be seen that the background estimation describes the data well.

11 Systematic uncertainties

Several possible sources for systematic uncertainties have been studied and estimated.

11.1 Signal yield uncertainties

The total systematic uncertainty of the signal yields is 6% on average. The sources and their individual contributions are described below.

- **Luminosity**

  An uncertainty of 3.4% was assumed [34].

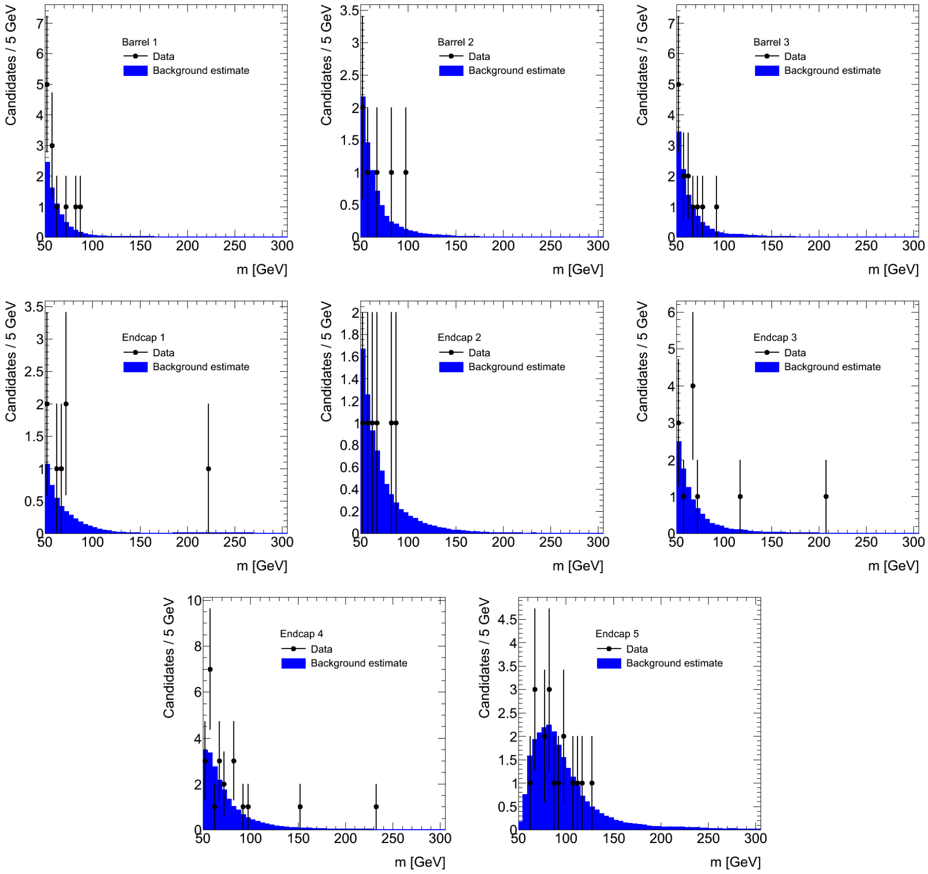

Figure 23: Measured mass (black) and background mass estimation in the different η regions in the slepton search. Candidates in these plots passed the selection criteria discussed in section 9.3.

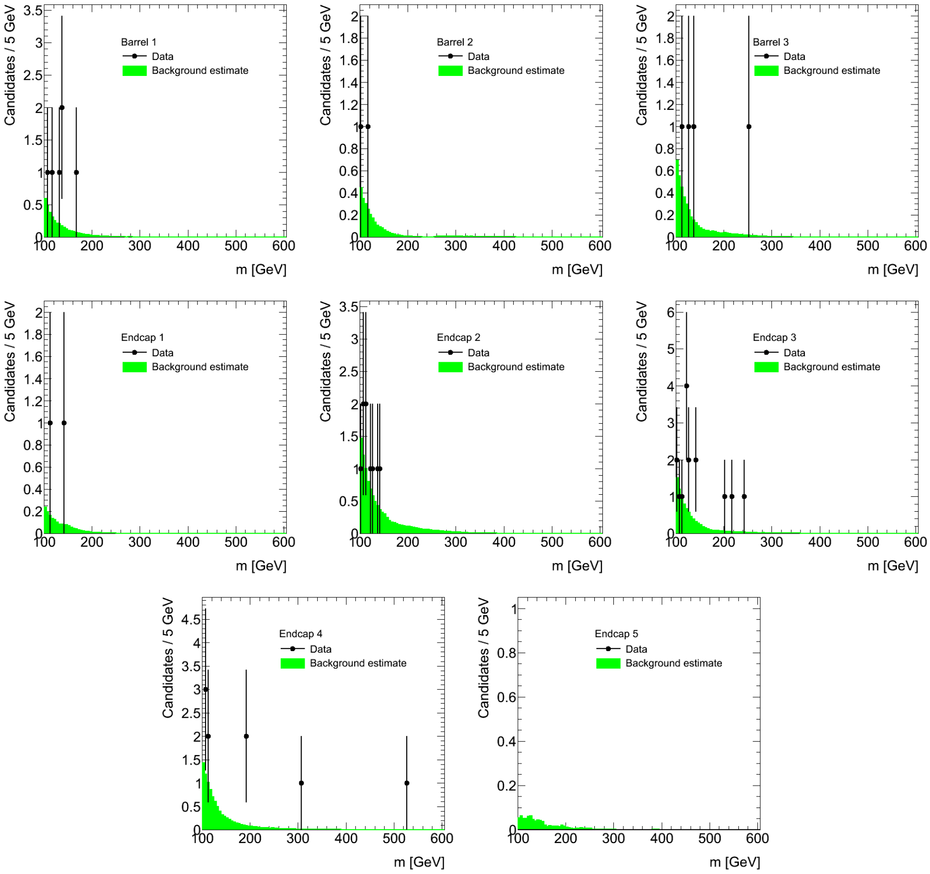

Figure 24: Measured mass (black) and background mass estimation in the different η regions in the R-hadron search. Candidates in these plots passed the selection criteria discussed in section 9.3.

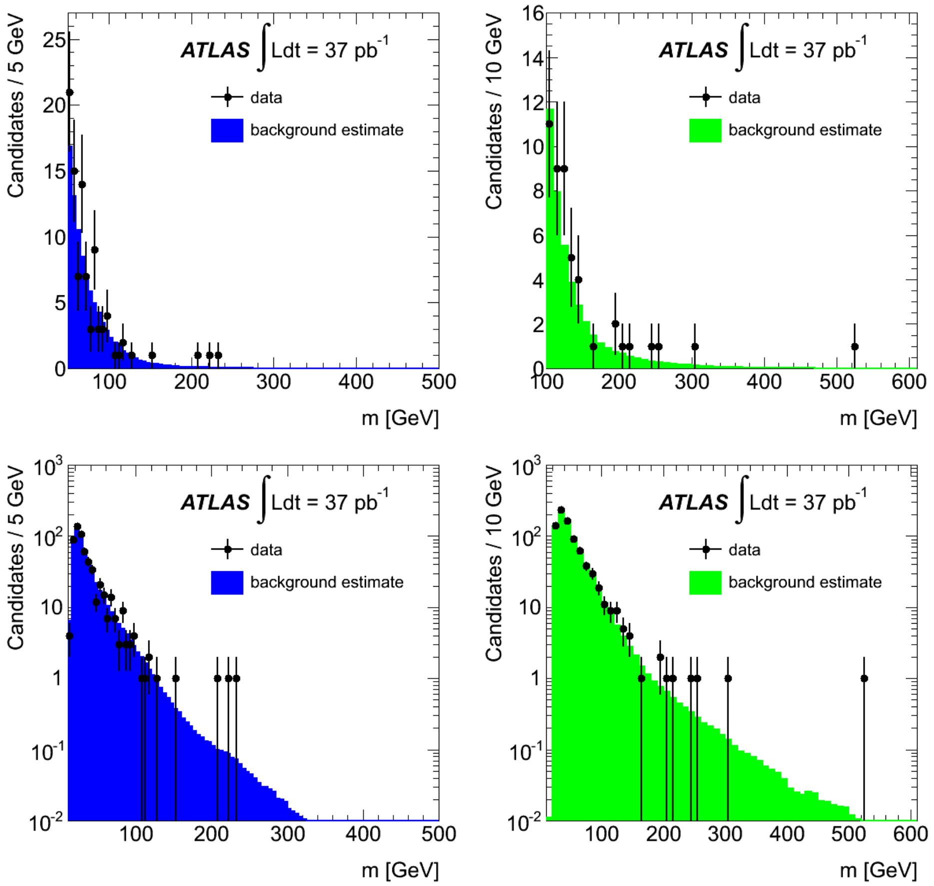

Figure 25: Measured mass (black) and background mass estimation, combined in all regions, in the slepton search (left) and R-hadron search (right). The full mass range is shown in log scale (top) and the high mass regions is shown in linear scale (bottom). Candidates in these plots passed the selection criteria discussed in section 9.3.

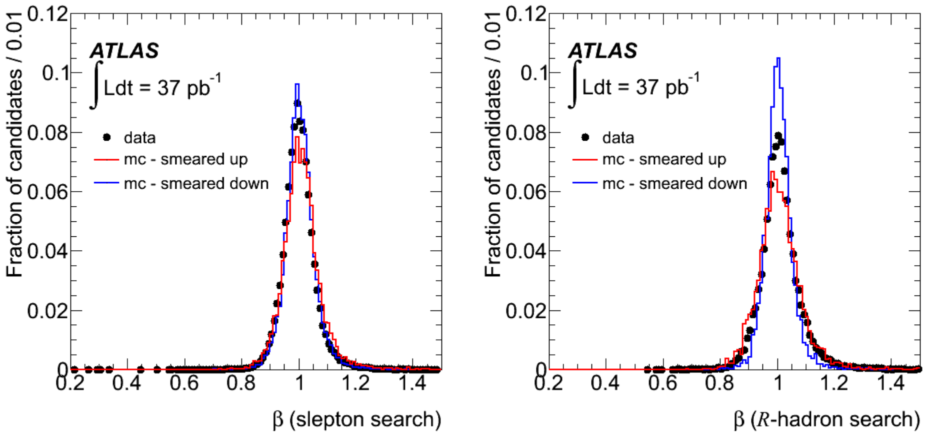

Figure 26: Muon β distribution in the data (black) and MC muons from Z decay smeared with up (red) and down (blue) smearing factor in the sleton (left) and R-hadron (right) searches.

- **Trigger**

  The systematic uncertainty associated with the trigger selection is estimated in [35] to be 0.73% (0.35%) and 0.74% (0.42%) in the barrel (endcap) for the two trigger chains used in the slepton search. An uncertainty of 5% is estimated for the R-hadron search. The trigger efficiency for particles arriving late at the MS is included in the simulation. Differences between data and Monte Carlo trigger efficiency due to the time resolutions were tested and are negligible.

- **Signal resolution expected in the data**

  As explained in section 8.6 the signal resolution expected in the data is estimated by smearing the hit times according to the current time calibration. The systematic uncertainty due to the smearing process is estimated by scaling the hit times smearing factor up and down by 10% for the slepton search and by 50% for the R-hadronsearch, so that they bracket the data β distribution. Figure 26 shows the muon β distribution in the data (black) and MC muons from Z decay smeared with up (red) and down (blue) smearing factors. The results are shown for the slepton (left) and R-hadron (right) searches.

  Examples of mass distributions smeared with central (black) up (red) and down (blue) smearing factors are shown in figure 27 for a $\tilde{\tau}$ with a mass of 116.3 GeV (left) and $\tilde{g}$ with a mass of 500 GeV (right). 6% (2%) systematic uncertainty is associated with the smearing process for the GMSB models in the barrel (endcap). For the $\tilde{g}$ R-hadrons, the smearing effect is within the statistical error of the generated sample

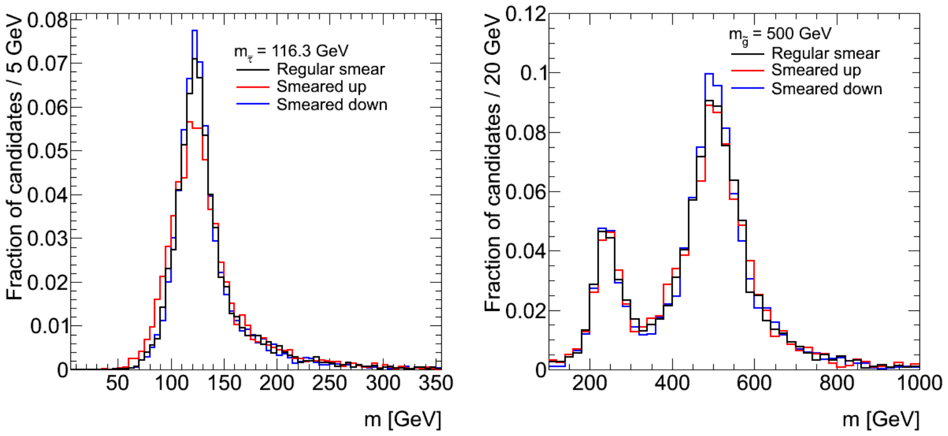

Figure 27: The mass distribution of $\tilde{\tau}$ with a mass of 116.3 GeV (left) and $\tilde{g}$ with a mass of 500 GeV smeared with central (black) up (red) and down (blue) factors.

size.

The systematic errors due to track reconstruction efficiency and momentum resolution differences between ATLAS data and simulation were estimated using standard ATLAS tools to be 0.5% for GMSB events and between 0.8% and 1.3% for R-hadron in the different hadronization and interaction models.

11.2 Background estimation uncertainties

Systematic uncertainties on the background estimation method are possible due to correlations between the β and momentum distributions of the candidates. Another systematic error on the background estimation arises from the limited statistics of the sample used to estimate the background. A total of 15% (20%) uncertainty is estimated for the slepton (R-hadron) search resulting from individual contribution discussed below.

The main source of systematic uncertainties on the background estimation is the variation of the β distribution within the different detector regions used in the background estimation. The analysis makes a cut on p_{T}, and therefore the momentum is correlated with η. If there are systematic differences in β distributions within each region, the background estimate could be sensitive to the cases where β from one part of a region is convoluted with momentum from another part.

To quantify the variations of the β distribution within a region and its effect on the background estimate, each region was sub-divided into smaller regions in which the β distribution was evaluated. The β distributions of the sub-regions were compared by their mean, and the variation of their

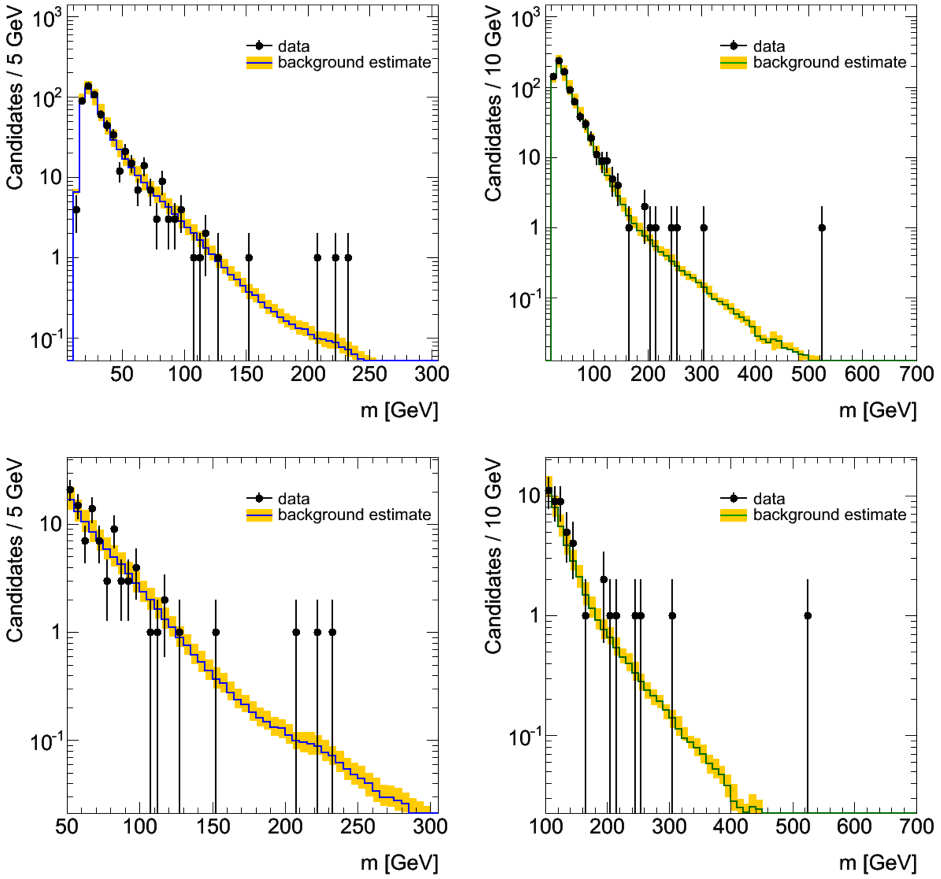

Figure 28: Background estimate (colored line) and the systematic uncertainty (yellow band) associated with it for the background estimate obtained in the slepton search (left) and in the R-hadron search. The full mass range is shown on top and the high mass region on the bottom.

mean was used as a variation estimate of the β distribution within a region. To derive the uncertainty bands caused by this, two background estimates were produced after shifting the β distribution of a region by the variability estimate. Figure 28 shows the background estimate (colored line) and the systematic uncertainty (yellow band) associated with it for the background estimate obtained in the slepton search (left) and in the R-hadron search. The full mass range is shown on top and the high mass region on the bottom.

Another systematic error arises if the β distribution depends on the candidate momentum. To test this, the candidates in each η region were divided by their momentum into two bins with similar counts and background estimates were produced using the β distribution of each momentum bin. The resulting background estimates are shown in figure 29 for the slepton (left)

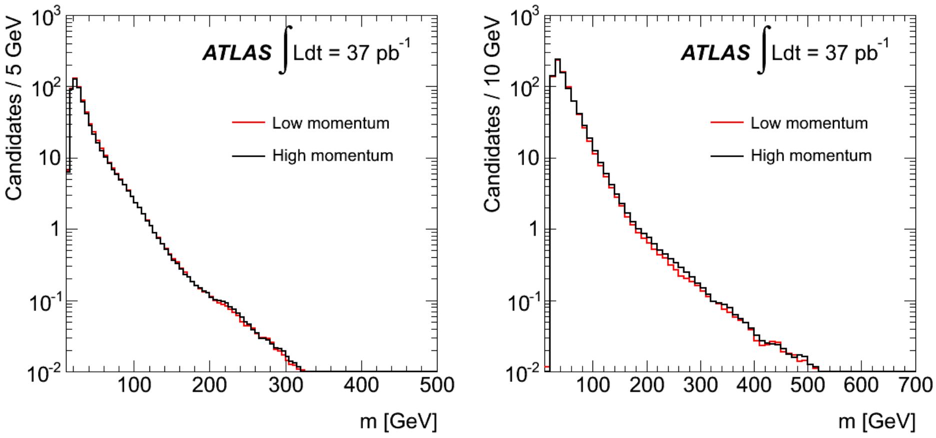

Figure 29: Background estimates produced with muon β p.d.f.'s of muons with high (black) and low (red) momenta. The distributions are shown for the slepton search (left) and for the R-hadron search (right).

and R-hadron (right) searches. It can be seen that this procedure produced a negligible systematic error, confirming that the β distribution of muons does not depend on their momentum.

Using the β distribution obtained from the $Z \rightarrow \mu\mu$ sample rather than the generic sample would test another systematic effect. It can be seen from figure 21 that the two distributions are similar, and indeed, the resulting systematic uncertainty was negligible.

Finally, the background estimation is based on a limited statistics sample, that of all candidates that passed the quality cuts, before the cut on β. The tail of the background mass distribution has a significant contribution from a few high momentum events, and a statistical error arises from this. In order to calculate the sensitivity of the limits obtained to the statistics of the momentum distribution, the candidate sample was divided randomly into two samples and the background estimate derived from each 1/2 sample separately. The difference between the two background estimates above each mass cut is multiplied by $\sqrt{2}$ giving the difference between the sample used in this analysis and a different sample of the same size. The resulting error on the slepton search ranges from 1.47 candidate for $M > 90$ GeV to 0.19 candidate for $M > 140$ GeV. The systematic errors on the R-hadron search background estimation arising from sample statistics are negligible at 0.05 candidate for $M > 250$ GeV and 0.06 candidate for $M > 350$ GeV. These numbers are used as the systematic uncertainty arising from the statistical error on the background estimate.

$M_{\tilde{\ell}}$	mass cut [GeV]	expected signal	expected background	data
101.9	90	35.9	19.2	16
116.3	110	13.6	9.8	8
131.0	120	7.3	7.2	5
160.7	130	2.0	5.4	4

Table 11: Slepton search mass cuts and expected and observed events with a candidate above it as a function of the $\tilde{\ell}$ mass

11.3 Theoretical cross-sections uncertainties

The PROSPINO program was used to calculate the cross sections at next to leading order and two sources of theoretical systematic uncertainties were considered; The renormalization and factorization scales are set to the average of the final state particle masses and are changed upward and downward by a factor of two. This results in a systematic error of 7% for GMSB cross-sections and 15% for gluino cross-sections [5]. The parton densities of CTEQ6.6 [36] functions were used. The systematic uncertainties on GMSB were estimated by applying the p.d.f. error function to the next to leading order cross section calculation, yielding a systematic uncertainty of about 5%. A variation of less than 5% was observed in [5] for R-hadrons when substituting the MSTW 2008 next to leading order p.d.f. set for CTEQ6.6.

12 Results

The CLs approach [37] for counting experiments is used to derive the limits for the production cross-section of GMSB and $\tilde{g}$ R-hadron events. The limits are obtained by comparing the expected number of events with a candidate above a given mass cut with the actual number of events with a candidate above the same mass cut observed in the data.

12.1 Mass cut determination

For each model, the mass cut was chosen to optimize the ratio between the expected number of candidates and the expected limit. This limit is obtained using the background estimation to derive the expected number of background events above the mass cut. Figure 30 shows these ratios for the different GMSB (left) and R-hadron (right) models. The selected mass cuts for the different models are summarized in tables 11 and 12 together with the observed data and expected signal and background in each case.

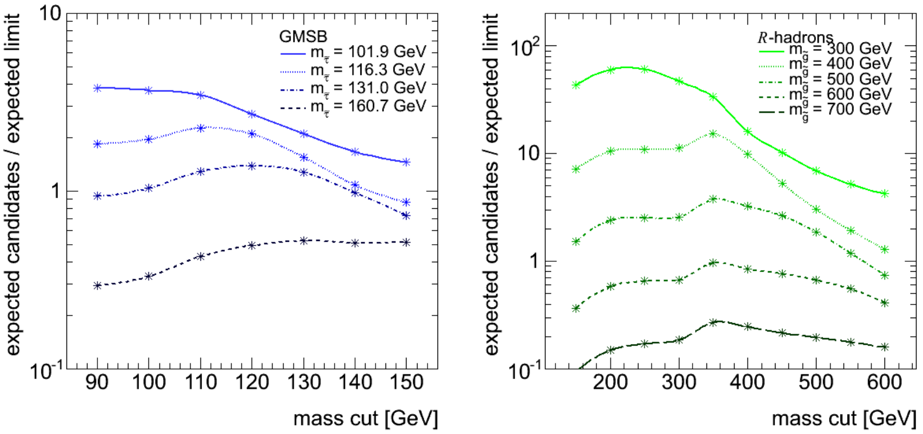

Figure 30: The ratio between the expected number of signal candidates and the expected lower limit as a function of the mass cut, for the slepton search (left) and R-hadron search (right).

$M_{\tilde{g}}$	mass cut [GeV]	expected signal	expected background	data
300	250	254.4	2.3	3
400	350	36.2	0.7	1
500	350	8.7	0.7	1
600	350	2.2	0.7	1
700	350	0.6	0.7	1

Table 12: R-hadron search analysis mass cuts and expected and observed events with a candidate above it as a function of the $\tilde{g}$ mass

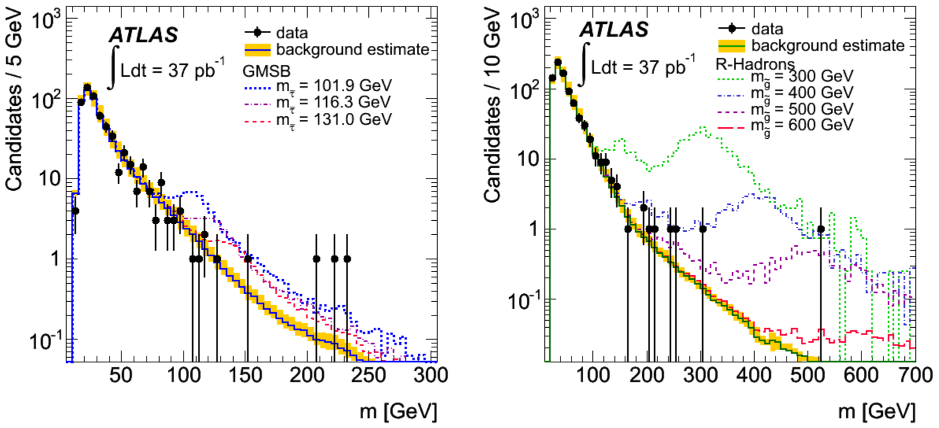

Figure 31: Candidate estimated mass distribution for data, expected background including systematic uncertainty, with simulated signals added, in the slepton (left) and R-hadron (right) searches.

12.2 Limits

The expected number of signal candidates in the dataset with integrated luminosity of 37 pb^{-1} is added to the background estimation and compared to the data in figure 31 for the different GMSB (left) and R-hadron (right) models. The production cross-section and cross-section limit at 95% CL is shown in figure 32, as a function of the $\tilde\tau$ mass for the slepton search (left) and as a function of the $\tilde g$ mass for the R-hadron search (right).

Stable $\tilde\tau$ are excluded at 95% CL up to a mass of 136 GeV, in GMSB models with $N_5 = 3$, $m_{\text{messenger}} = 250$ TeV, sign$(\mu) = 1$ and tan$\beta = 5$. The sensitivity of these limits to the SUSY parameters are reduced in two ways; Figure 33 (left) shows the limit obtained for sleptons produced in electroweak processes only, which have small dependence on model parameters besides the slepton mass. Electroweakly produced sleptons are excluded at 95% CL up to a mass of 110 GeV.

Figure 33 (right) shows the cross-section limits for sleptons passing the fiducial cuts $p_{\mathrm{T}} > 40$ and $|\eta| < 2.5$ at the generator level. The resulting efficiencies as a function of β, p_{T}, η and ϕ are shown in figure 34. It should be noted that the cut on p_{T} creates a mass dependent effective cut at low β. The cut at $\beta < 0.95$ creates a mass dependent effective cut at high p_{T} and was not included in the efficiency plots below. In addition, due to resolution, some candidates with generated $\beta > 0.95$ are selected in the analysis. The fraction of sleptons with reconstructed $\beta < 0.95$ is within 1% of those with generated $\beta < 0.95$ for all studied models.

These limits are only applicable to models where the $\tilde\tau$ or $\tilde\ell$ are the NLSP, and their lifetime is sufficiently long to traverse the ATLAS experiment and

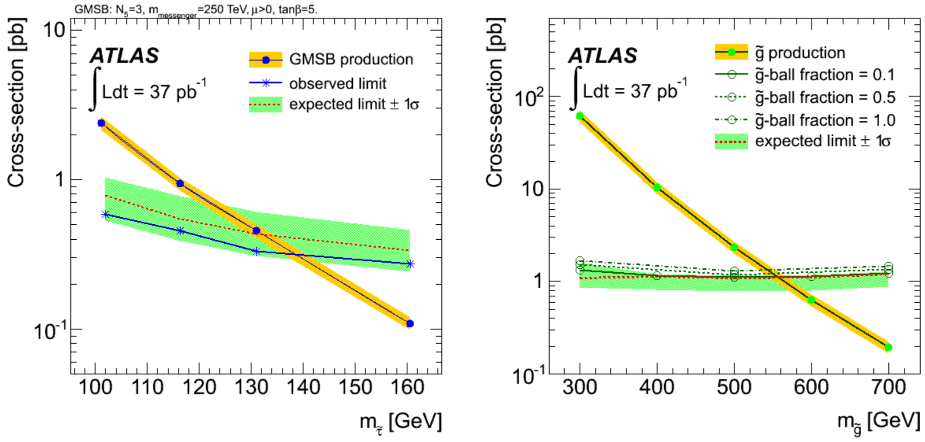

Figure 32: The production cross-section and cross-section limit at 95% as a function of the $\tilde{\tau}$ mass for the slepton search (left) and as a function of the $\tilde{g}$ mass for the R-hadron search (right). Cross-section uncertainties are shown as yellow bands. The median expected limit is marked with dashed red line. The green band is the 1σ variation of the expected limit.

reach the MS. In this case, the limits obtained for the above models should have little dependence on $\tan\beta$ and N_5.

$\tilde{g}$ R-hadron in the generic scattering model described in [19] are excluded at 95% CL up to a mass of 544 GeV. The 95% CL limits for $\tilde{g}$ R-hadrons with the scattering model described in [20] and [21] are 494 GeVand 439 GeV respectively. The limits in these models are lower since smaller fraction of R-hadrons are charged in the MS. Since the R-hadron search does not require the existence of an ID track, the selection efficiency is affected very little by the $\tilde{g}$-ball fraction. The small difference between the models with different fractions is due to the primary vertex and z_0 requirement in the event selection criteria discussed in 9.3. Generic scattering models with $\tilde{g}$-ball fractions of 0.5 and 1.0 are excluded at 95% CL up to masses of 537 GeVand 530 GeVrespectively.

13 Summary and conclusion

A search for long-lived charged particle reaching the MS was performed with 37pb^{-1} of data collected with the ATLAS detector. No excess was observed above the expected background estimation. Stable $\tilde{\tau}$ are excluded at 95% CL up to a mass of 136 GeV, in GMSB models with $N_5 = 3$, $m_{\text{messenger}} = 250$ TeV, sign$(\mu) = 1$ and $\tan\beta = 5$. Gluino R-hadron in the generic interaction model described in [19] are excluded up to masses of 530 GeV to 544 GeV, where the range spans the full range of $\tilde{g}$-ball fractions.

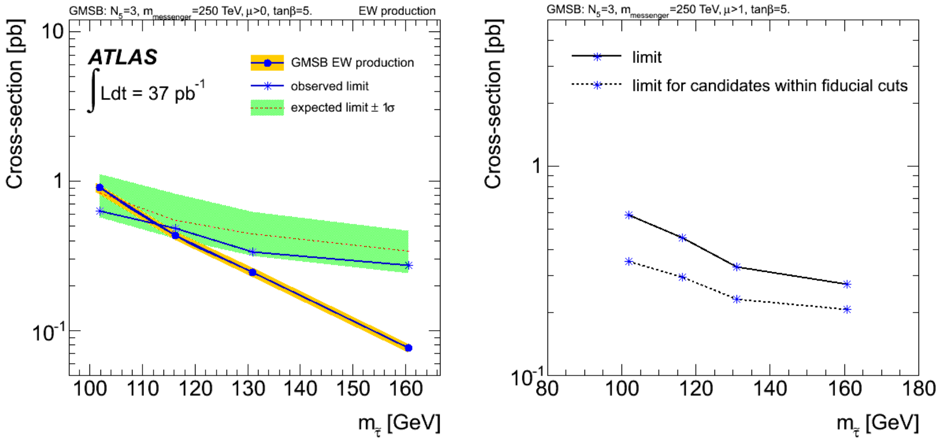

Figure 33: The production cross-section and cross-section limit at 95% as a function of the slepton mass for sleptons produced in electroweak processes only (left) and for sleptons passing he fiducial cuts $p_{\mathrm{T}} > 40$,$|\eta| < 2.5$ and $\beta < 0.95$ at the generator level. Cross-section uncertainties are shown as yellow bands. The median expected limit is marked with dashed red line. The green band is the 1σ variation of the expected limit.

References

[1] Yu.A. Golfand and E.P. Likhtman, JETP Lett. 13 (1971) 323.

A. Neveu and J.H. Schwartz, Nucl. Phys. B31 (1971) 86.

A. Neveu and J.H. Schwartz, Phys. Rev. D4 (1971) 1109.

P. Ramond, Phys. Rev. D3 (1971) 2415.

D.V. Volkov and V.P. Akulov, Phys. Lett. B46 (1973) 109.

J. Wess and B. Zumino, Phys. Lett. B49 (1974) 52.

J. Wess and B. Zumino, Nucl. Phys. B70 (1974) 39.

[2] The LHC Study Group, *The Large Hadron Collider Accelerator Project*, CERN/AC/93-03(LHC), 1993.

[3] M. Dine, W. Fischler and M. Srednicki, Nucl. Phys. B189, 575 (1981).

S. Dimopoulos and S. Raby, Nucl. Phys. B192, 353 (1981).

C. Nappi and B. Ovrut, Phys. Lett.113B, 175 (1982).

L. Alvarez-Gaume, M. Claudson and M. Wise, Nucl. Phys. B207, 96 (1982).

M. Dine and A. Nelson, Phys. Rev. D48, 1227 (1993).

M. Dine, A. Nelson and Y. Shirman, Phys. Rev. D51, 1362 (1995).

M. Dine, et al., Phys. Rev. D53, 2658 (1996).

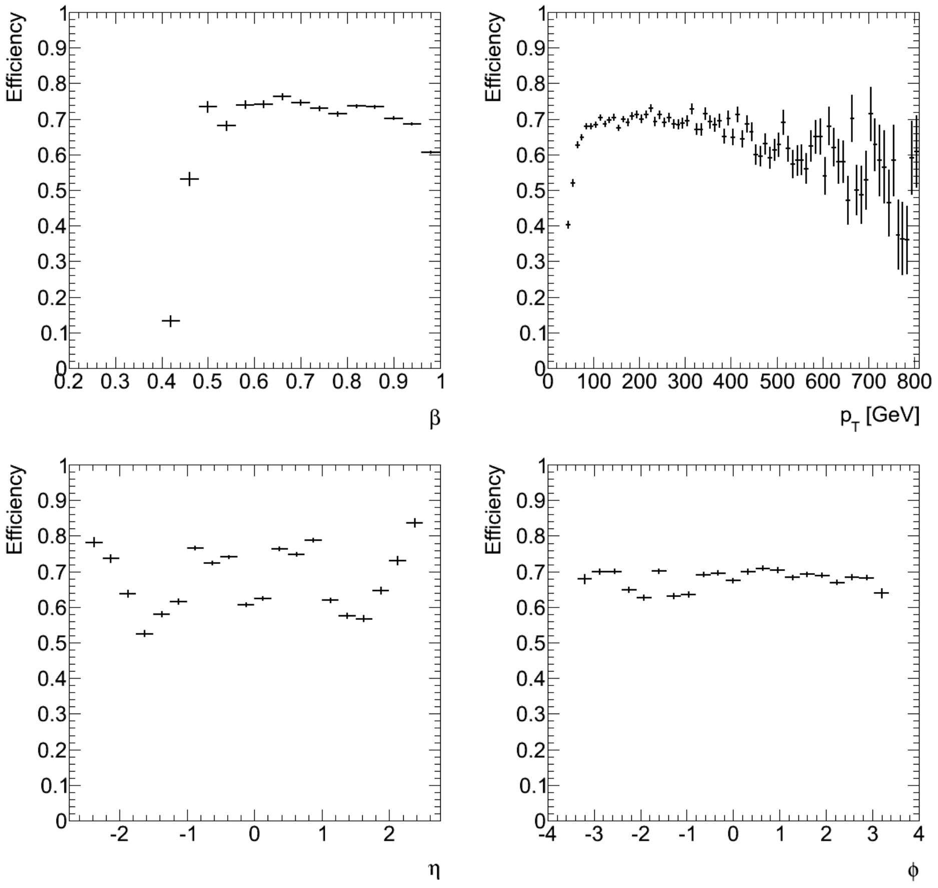

Figure 34: The candidate selection efficiency with respect to candidates passing the cuts $p_{\mathrm{T}} > 40$ and $|\eta| < 2.5$ at the generation level. The selection efficiency is shown as a function of β, p_{T}, η and ϕ.

[4] G.F. Giudice, R. Rattazzi, *Theories with Gauge-Mediated Supersymmetry Breaking*, Phys. Rep. **322** (1999) 419-499.

[5] D. Casadei, et al, *Search for Stable Hadronising Squarks and Gluinos at the ATLAS Experiment at the LHC*, submitted to Phys. Lett. B.

[6] N. Arkani-Hamed, S. Dimuoulus, G. R. Dvali, Phys. Rev. D (1999).

[7] G.F Giudice, A. Romanio, hep-ph/0406688v2 (2004).

[8] S. Weinberg, Phys. Rev. D 13, 974 (1976), Phys. Rev. D 19, 1277 (1979).

E. Gildener, Phys. Rev. D 14, 1667 (1976).

L. Susskind, Phys. Rev. D 20, 2619 (1979).

G. 't Hooft, *in Recent developments in gauge theories, Proceedings of the NATO Advanced Summer Institute, Cargese 1979, (Plenum, 1980).*

[9] M. Fairbairn, et al., *Stable massive particles at colliders* , phys. Rept. 438 (2007) 1-63. arXiv:hep-ph/0611040.

[10] I. Hinchliffe, F. E. Paige, *Measurements in Gauge Mediated SUSY Breaking Models at LHC /}, (1998), arxiv:hep-ph/9812233*

[11] J. L. Feng, T. Moroi, *Tevatron signatures of longlived charged sleptons in gauge mediated supersymmetry breaking models./}, Phys.Rev.D58:035001 (1998).*

[12] H. Baer, K Cheung, J.F. Guinion, Phys. Rev. 59.

[13] ATLAS Collaboration, *The ATLAS Experiment at the CERN Large Hadron Collider*, JINST 3 (2008).

[14] ATLAS Level-1 Trigger Group, *Level-1 Technical Design Report*, ATLAS TDR 12, Aug., 1998.

[15] ATLAS HLT/DAQ/DCS Group, *High-Level Trigger, Data Acquisition, and Control Technical Design Repor*, ATLAS TDR 16, Nov., 2002.

[16] ATLAS Muon Collaboration, *ATLAS Muon Spectrometer Technical Design Report*, CERN/LHCC 97-22, June, 1997.

[17] ATLAS Collaboration,*Muon reconstruction efficiency in reprocessed 2010 LHC proton-proton collision data recorded with the ATLAS detector*,ATLAS-CONF-2011-063, Apr., 2011.

[18] ATLAS collaboration,*Readiness of the ATLAS Tile Calorimeter for LHC collisions*, EPJC 70 (2010) 1193.

[19] R. Mackeprang, A. Rizzi, *Interactions of Coloured Heavy Stable Particles In Matter*, Eur.Phys.J.C50 (2007) 353-362.

A. C. Kraan, *Interactions of heavy stable hadronizing particles*, Eur. Phys. J. C37 (2004) 91-104.

[20] R. Mackeprang, D. Milstead, *An Updated Description of Heavy-Hadron Interactions in GEANT-4*, Eur. Phys. J. C66 (2010) 493-501.

[21] G. Farrar, R. Mackeprang, D. Milstead, J. Roberts, *Limit on the mass of a long-lived or stable gluino*, JHEP 1102 (2011) 018.

[22] M. Fairbairn, et al, hep-ph/0611040v2 (2006).

[23] A. Mafi, S. Raby, Phys. Rev. D 62 (2000).

[24] W. Beenakker, R. Hopker, and M. Spira, (1996) arXiv:hep-ph/9611232.

[25] G. Engelhard, J. L. Feng, I. Galon, D. Sanford, Y. Felix, *SPICE: Simulation Package for Including Flavor in Collider Events*, arXiv:0904.1415 [hep-ph].

[26] G. Corcella, I.G. Knowles, G. Marchesini, S. Moretti, K. Odagiri, P. Richardson, M.H. Seymour and B.R. Webber, *HERWIG 6.5*, JHEP 0101 (2001) 010 [hep-ph/0011363]; hep-ph/0210213.

[27] S. Agostinelli et al., *GEANT4: A simulation toolkit*, Nucl. Instrum. Meth. A506 (2003) 250-303.

[28] The ATLAS Collaboration, *The ATLAS Simulation Infrastructure*, Eur. Phys. J. C70 (2010) 823-874. arXiv:1005.4568.

[29] T. Sjostrand, S. Mrenna, P. Skands, *PYTHIA 6.4 Physics and Manual*, JHEP 05 (2006) 026. arXiv:hep-ph/0603175.

[30] R. Mackeprang, D. Milstead, *An Updated Description of Heavy-Hadron Interactions in GEANT-4*, Eur. Phys. J. C66 (2010) 493-501. arXiv:0908.1868.

[31] S. Tarem, Z. Tarem, N. Panikashvili, O. Belkind, *MuGirl - Muon identification in ATLAS from the inside out*, Nuclear science symposium conference record, 2006. IEEE VOLUME 1, may 2007, pages 617 - 621.

[32] S. Tarem, S. Bressler, H. Nomoto, A. Di Mattia, *Trigger and reconstruction for a heavy long lived charged particles with the ATLAS detector*, The European Physical Journal C **62** (2009) 281.

[33] J. Kiefer, *Sequential minimax search for a maximum*, Proceedings of the American Mathematical Society 4 (3), (1953).

[34] The ATLAS Collaboration, *Updated Luminosity Determination in pp Collisions at* $\sqrt{s} = 7$ *TeV using the ATLAS Detector*, ATLAS-CONF-2011-011.

[35] ATLAS Collaboration, *Measurement of the Muon Charge Asymmetry from W Bosons Produced in pp Collisions at* $\sqrt{s} = 7$ *TeV with the ATLAS detector*, Mar 2011, arXiv:hep-ex/hep-ex1103.2929.

[36] J. Pumplin et al., JHEP 07 (2002) 012.

[37] A. L. Read, *Modified frequentist analysis of search results (the* CL_s *method)* CERN-OPEN-2000-205 (2000).